Forschungszentrum Karlsruhe
Technik und Umwelt

Wissenschaftliche Berichte
FZKA 5681

On the Diffraction of Harmonic Spherical Waves: A Comparison between the Strict Sommerfeld Description and the Ray Tube Approximation

S. Honcu, M. Krauß, Ch. Weddigen

Institut für Meteorologie und Klimaforschung
Hauptabteilung Daten- und Informationsverarbeitung

Dezember 1995

Forschungszentrum Karlsruhe
Technik und Umwelt
Wissenschaftliche Berichte
FZKA 5681

On the Diffraction of Harmonic Spherical Waves: A Comparison between the Strict Sommerfeld Description and the Ray Tube Approximation

S. Honcu, M. Krauß, Ch. Weddigen

Institut für Meteorologie und Klimaforschung
Hauptabteilung Daten- und Informationsverarbeitung

Forschungszentrum Karlsruhe GmbH, Karlsruhe
1995

Forschungszentrum Karlsruhe GmbH
Postfach 3640, 76021 Karlsruhe

ISSN 0947-8620

Abstract

The diffraction is investigated of harmonic spherical scalar waves without attenuation at the plane interface between two homogeneous fluids. For the strict Sommerfeld integral description and for the ray tube approximation numerical examples, calculated for the near field region, are figured in two-dimensional plots of the reflected and transmitted wave fields. Ratios of densities and phase velocities are chosen such that the results could be extended to describe the diffraction of electromagnetic dipole waves. A special mechanism of phase angle absorption of a wave field transmitted into an acoustically thinner medium has been found which to our knowledge has not yet been described in the literature.

Zur Berechung harmonischer sphärischer Wellen: Ein Vergleich zwischen der exakten Beschreibung nach Sommerfeld und der Näherung der geometrischen Akustik

Zusammenfassung

Die Brechung von harmonischen sphärischen skalaren Wellen ohne Absorption an einer ebenen Trennfläche zwischen zwei homogenen Fluiden wird untersucht. Numerische Beispiele werden zweidimensional dargestellt für reflektierte und transmittierte Wellen im Nahfeldbereich, und zwar für die exakte Integralmethode nach Sommerfeld und für die Näherung der geometrischen Akustik (ray tube approximation). Die Verhältnisse von Dichten und Phasengeschwindigkeiten wurden so gewählt, daß die Ergebnisse auch zur Beschreibung der Brechung elektromagnetischer Dipolwellen dienen können. Ein spezieller Mechanismus zur Phasenwinkelabsorption im Feld einer in ein akustisch dünneres Medium transmittierten Welle wurde gefunden, der - nach unserer Kenntnis - bisher in der Literatur noch nicht beschrieben wurde.

Table of Contents

1. Introduction

Atmospheric emission measurements, which were performed with the airborne variant of the Michelson Interferometer of Passive Atmospheric Sounding (MIPAS, [1]) under the German stratospheric ozone program from 1991 until 1995, revealed heavily disturbed phase and magnitude spectra. These disturbances were attributed [2, 3] to thermally excited dipole radiation from sources within the beam splitter. Since, for a quantitative treatment, multiple reflections and transmissions at the surfaces of the beam splitter are needed, the strict Sommerfeld description [4] should be used in a first step which, of course, was not practicable in our case. Therefore, for the semiquantitative treatment in ref. [2] , the Ray Tube Approximation (RTA) was supposed to be valid which describes the diffraction of divergent rays by the Fresnel coefficients for plane waves. This might be a good approximation in the far field region of an electromagnetic dipole, but certainly not for distances z_0 of the source from the diffracting plane which are comparable with or smaller than the wavelength. This is the case for thermal beam splitter emission.

The refraction of electromagnetic dipole radiation is closely related to the refraction of scalar spherical waves like acoustic waves in fluids (see e.g. ref. [5], p. 79 ff). The sound pressure p can be used to form the Hertz vector $\vec{\Pi}_e = p\vec{n}$ ($\vec{n}$ is the unit vector in the direction of the oscillating dipole) from which, by differential operations, the electric and magnetic fields of the diffracted wave can be derived.

As a first step towards a quantitative description of beam splitter emission we prepared the mathematical and computational tools for numerical calculations needed to compare the strict Sommerfeld solution with the RTA results. In Section 2 of this report we will summarize the diffraction of harmonic scalar plane waves defining quantities which will be needed later. In Section 3 complex and real expressions for the strict Sommerfeld description will be given. Before proceding to the RTA, we will introduce 'optical' coordinates, which in our case are suited to formulate RTA expressions. Finally, some typical results of the strict Sommerfeld method will be indicated and compared with those from the RTA.

In this report we will restrict ourselves to harmonic scalar waves without attenuation. For the sake of simplicity different quantities will occasionally be described by the same symbol, but only if there is no risk of confusion.

2. The Diffraction of Plane Waves

The diffraction of scalar harmonic acoustic plane waves has been described by Bretkovistikh and Godin [6] . We summarize here the results as far as they will be needed in the subsequent sections.

2.1 The Helmholtz equation

The sound pressure $p(\vec{r},t)$ in isotropic fluids (gases or liquids) without attenuation and at rest is described in an adiabatic and linear approximation by the wave equation

$$\frac{\partial^2 p(\vec{r},t)}{\partial t^2} - c^2 \Delta p(\vec{r},t) = 0 \quad , \tag{2.1}$$

where $c = (\xi/\rho)^{1/2}$ is the phase velocity of sound (ρ = *density*, ξ = *compressibility*). For harmonic waves $p(\vec{r},t) = p(\vec{r})\, e^{-i\omega t}$ with the angular frequency ω . In a source free region the phasor $p(\vec{r})$ satisfies the homogeneous Helmholtz equation

$$\Delta p(\vec{r}) + k^2 p(\vec{r}) = 0 \ , \tag{2.2}$$

where $k = \omega/c$ is the scalar wave number and Δ is the Laplace operator. From now on, we will call $p(\vec{r})$ sound pressure or simply pressure. The general solution of Eq. (2.2) for plane waves with $\partial/\partial y = 0$ (omitting coordinate and time independent factors) is

$$p(\vec{r}) = e^{i\vec{k}\vec{r}} \ , \tag{2.3}$$

where the vector $\vec{k} = (k_x, 0, k_z)$ of the wave number satisfies

$$\vec{k}^2 = k^2 \ . \tag{2.4}$$

The vector $\vec{k}$ may be real or complex which leads to the following two types of plane waves.

2.1.1 Homogeneous plane waves

If $\vec{k}$ is real, the pressure is given by

$$p(\vec{r}) = e^{i(k_x x + k_z z)} \quad . \tag{2.5}$$

The absolute value of $p(\vec{r})$ is constant. This type is called homogeneous because planes of constant phase are also planes of constant intensity (see Fig. 1).

2.1.2 Inhomogeneous plane waves

If we allow $\vec{k}$ to be complex ($\vec{k} = \vec{k}_1 + i\,\vec{k}_2$, $\vec{k}_1$, $\vec{k}_2 = real$), it follows from (2.4) that

$$\vec{k}_1\vec{k}_2 = 0 \quad , \quad \vec{k}_1^2 - \vec{k}_2^2 = k^2 \quad . \tag{2.6a, b}$$

Then the pressure becomes

$$p(\vec{r}) = e^{-\vec{k}_2\vec{r}}\, e^{i\vec{k}_1\vec{r}} \quad . \tag{2.7}$$

The wave number of the oscillating part is increased with respect to k, and the absolute value of $p(\vec{r})$ decreases exponentially in a direction perpendicular to $\vec{k}_1$ (see Fig 1b). From

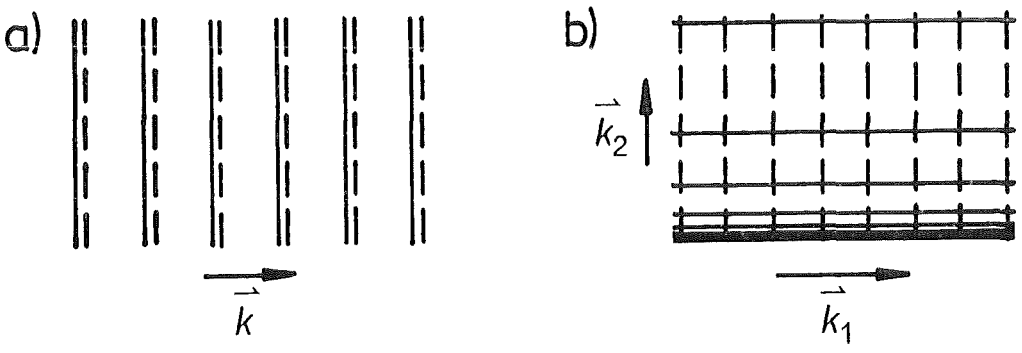

Fig.1: Homogeneous (a) and inhomogeneous (b) plane waves. Solid lines indicate planes of constant intensity, broken lines planes of constant phase.

optics we know this case as transversely attenuated waves [7] which, when total reflection occurs, penetrate into the optically thinner medium and propagate parallel to the interface.

2.2 *Boundary conditions*

If an incident wave

$$p_i(\vec{r}) = e^{ik(x\sin\theta - z\cos\theta)} \tag{2.8}$$

hits the plane interface between two isotropic fluids, a reflected wave p_r and a transmitted wave p_t will arise:

$$p_r(\vec{r}) = V\, e^{ik(x\sin\theta_r + z\cos z\theta_r)}\ , \tag{2.9}$$

$$p_t(\vec{r}) = W\, e^{ik_1(x\sin\theta_1 - z\cos\theta_1)}\ . \tag{2.10}$$

For definitions see Fig. 2. The Fresnel coefficients V for reflection and W for transmission and the relevant angles result from the boundary conditions at $z = 0$:

The ***kinematic boundary condition***

$$p_i(z=0) + p_r(z=0) = p_t(z=0) \tag{2.11}$$

calls for continuity of the pressure at the interface and leads to the Snellius refractive laws (equal phase in x-direction)

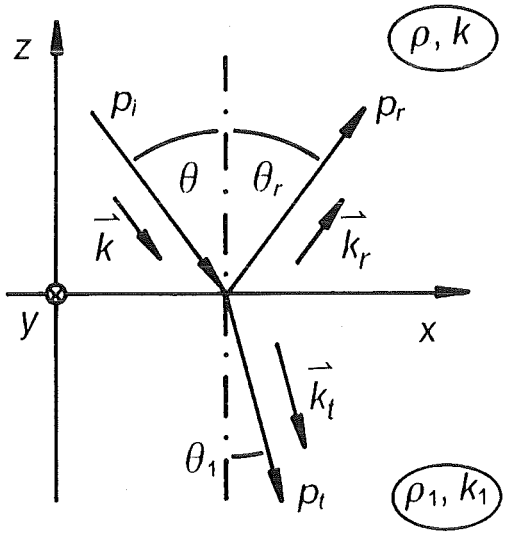

Fig.2: Refraction of an incident plane wave (p_i) at the interface of two homogeneous fluids. p_r, p_t are the reflected and transmitted waves. ρ, ρ_1 = *densities*, k, k_1 = wave numbers.

$$\theta_r = \theta, \quad \frac{\sin\theta}{\sin\theta_1} = \frac{k_1}{k} = n \ , \tag{2.12a, b}$$

and to a first relation between the Fresnel coefficients:

$$1 + V = W \ . \tag{2.13}$$

The ***dynamic boundary condition***

$$\frac{1}{\rho}\left(\frac{\partial p_i}{\partial z} + \frac{\partial p_r}{\partial z}\right) = \frac{1}{\rho_1}\frac{\partial p_t}{\partial z} \tag{2.14}$$

at $z = 0$ calls for equal accelerations and, therefore, for equal velocities and deviations in z-direction for the two media. The application of (2.14) to (2.9) and (2.10) gives the second condition for V and W:

$$m(1 - V)\cos\theta = nW\cos\theta_1 \ , \tag{2.15}$$

where $m = \rho_1/\rho$ is the ratio of densities and n is the relative refractive index (see Eq. 2.12b).

2.3 *The Fresnel coefficients*

From Eqs. (2.13) and (2.15) one obtains

$$V = \frac{m\cos\theta - n\cos\theta_1}{m\cos\theta + n\cos\theta_1} \ , \tag{2.16}$$

$$W = \frac{2m\cos\theta}{m\cos\theta + n\cos\theta_1} \ . \tag{2.17}$$

The value of V depends on m and n and on the angle θ of incidence. It varies within the limits shown in Fig. 3. The limiting cases $m = \infty$ (absolutely rigid) and $m = 0$ (absolutely soft) are treated in the literature for various scattering geometries, e.g. in Ref. [8] . The corresponding values are (V,W) = (1,2) and (-1,0), respectively.

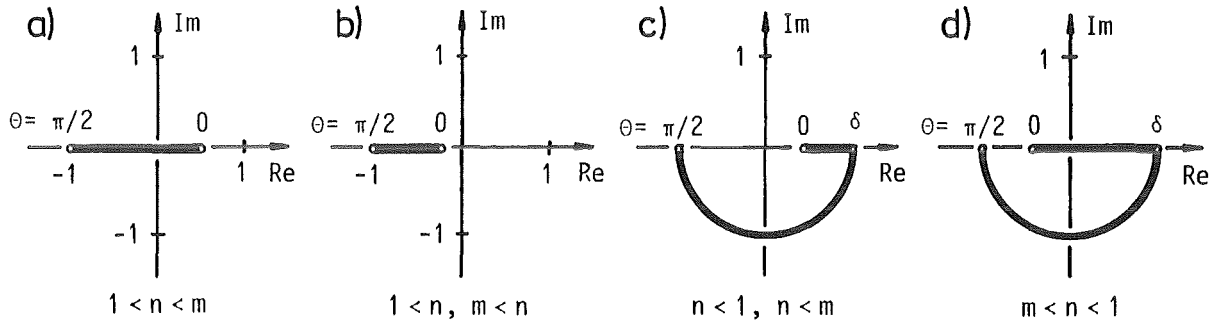

Fig.3: Real and imaginary parts of the reflection coefficient V (from [6] , p.23). Characteristic values for the angle θ of incidence are given. If θ exceeds δ , total reflection occurs and V gets complex. m = density ratio, n = relative refractive index.

It should be mentioned that the Fresnel coefficients for electromagnetic plane waves are obtained from the formal substitutions $m = \mu_1/\mu$ for the transverse electric (TE) case and $m = \varepsilon_1/\varepsilon$ for the transverse magnetic (TM) case. The meaning of n as the ratio of phase velocities $c = (\mu\varepsilon)^{-1/2}$ is unchanged (ε = *susceptibility*, μ = *permeability*). Since in most cases the deviation of μ from unity is negligible, (2.16) and (2.17) are valid for such waves if we write for

$$TE:\ m = 1, \qquad TM:\ m = n^2 \ . \tag{2.18a, b}$$

This means that TE waves behave according to Fig. 3b and 3c, whereas TM waves behave according to Fig. 3a and 3d. (Only for TM waves a Brewster angle with V = 0 exists.)

2.4 *Conservation of energy flux at the interface*

The specific mean energy flux density $\vec{I}$ of a harmonic scalar plane wave of unit amplitude is given by ([6] ,p. 19)

$$\vec{I} = \frac{\vec{k}}{2\rho c k} \ . \tag{2.19}$$

At an element dF of the interface, the energy fluxes for the incident, the reflected and the transmitted beams are

$$I_i dF = \frac{1}{2\rho c} \cos\theta dF \ , \tag{2.20}$$

$$I_r dF = \frac{1}{2\rho c} V \cos\theta dF \ , \tag{2.21}$$

$$I_t dF = \frac{1}{2\rho c} W \cos\theta_1 dF \ . \tag{2.22}$$

Conservation of energy flux means that

$$I_i dF = I_r dF + I_t dF \ . \tag{2.23}$$

If the Fresnel coefficients are taken from (2.16) and (2.17), relation (2.23) leads to the mathematical identity

$$m(1 - (\frac{m\cos\theta - n\cos\theta_1}{m\cos\theta + n\cos\theta_1})^2)\cos\theta = n(\frac{2m\cos\theta}{m\cos\theta + n\cos\theta_1})^2 \cos\theta_1 \ . \tag{2.24}$$

This means that the Fresnel coefficients describe the conservation of energy flux. This seems to be trivial, but is rarely described in textbooks. It will be explicitly needed for the ray tube approximation.

3. The Diffraction of Spherical Waves

Also the diffraction of spherical waves has been described by Brekhoviskitch and Godin [9]. They use the complex Sommerfeld formalism. To save computer time for numerical calculations, we transformed the complex formalism into a real one with reduced variables. An intermediate transformation of coordinates helps to simplify expressions.

3.1 The Sommerfeld integral description

In this report we choose the geometrical conditions shown in Fig. 4a. We start the derivation of the Sommerfeld description in Cartesian coordinates and then change over to cylindrical coordinates, as Sommerfeld did.

3.1.1 The incident wave

The sound pressure of a point source located at the Cartesian coordinates $(0,0, z_0)$ is given by

$$p(x,y,z) = \frac{e^{(ik\sqrt{x^2+y^2+(z-z_0)^2})}}{\sqrt{x^2+y^2+(z-z_0)^2}} \quad . \tag{3.1}$$

The Fourier transform of this expression for $z = z_0$ is proportional to $\exp(i(k_x x + k_y y))/\sqrt{k^2 - k_x^2 - k_y^2}$, where $\vec{k} = (k_x, k_y, k_z)$ is the vector of the wave number in the Cartesian k-space. Its backtransformation gives

$$p(x,y,z_0) = \frac{i}{2\pi}\int_{-\infty}^{+\infty}\int_{-\infty}^{+\infty} dk_x dk_y \exp(i(k_x x + k_y y))/\sqrt{k^2 - k_x^2 - k_y^2} \quad , \tag{3.2a}$$

$$Im(\sqrt{k^2 - k_x^2 - k_y^2}) \geq 0 \quad . \tag{3.2b}$$

The integrand of (3.2a) is a plane wave perpendicular to the z-axis.

The integral form of (3.1) for $z \neq z_0$ is obtained, if the integrand in (3.2a) is expanded by the factor $\exp(i\sqrt{k^2 - k_x^2 - k_y^2}\,|z - z_0|)$:

$$p(x,y,z) = \frac{i}{2\pi}\int_{-\infty}^{+\infty}\int_{-\infty}^{+\infty} \frac{dk_x dk_y}{\sqrt{k^2 - k_x^2 - k_y^2}} e^{(i(k_x x + k_y y + \sqrt{k^2 - k_x^2 - k_y^2}\,|z - z_0|))} \quad . \tag{3.3}$$

The integrand in this expression fulfills the Helmholtz equation (2.2), and for $z = z_0$ (3.3) equals (3.2a). The absolute value of $z - z_0$ must be used to avoid divergencies. If we pass to cylindrical coordinates in $\vec{r}$ – *space* and $\vec{k}$ – *space* and integrate over the azimuthal angle, we get the Sommerfeld integral representation

$$p_i(r,z,\varphi) = i\int_0^{\infty} \frac{k_r dk_r}{\sqrt{k^2 - k_r^2}} J_0(k_r r) e^{(i\sqrt{k^2 - k_r^2}\,|z - z_0|)} \quad . \tag{3.4}$$

Here, $k_r = \sqrt{k_x^2 + k_y^2}$ is the radial wave number and J_0 is the ordinary Bessel function of order zero:

$$J_0(u) = \frac{2}{\pi} \int_0^1 \frac{\cos(ut)}{\sqrt{1-t^2}}\, dt \quad , \tag{3.5}$$

$$\lim_{u \to \infty} J_0(u) \;=\; \sqrt{\frac{2}{\pi u}}\, \cos(u - \frac{\pi}{4}) \; . \tag{3.6}$$

In (3.4) the pressure was marked by a subscript i since it describes the incident wave for our geometry (Fig. 4a). Due to the axial symmetry we will suppress the azimuthal variable φ in the following relevant expressions.

3.1.2 The reflected and transmitted waves

To describe these waves we must expand the integrand of (3.4) by V (Eq. (2.16)) or W (Eq.(2.17)), expressed in k-coordinates (see Fig. 4b), and rearrange the exponent such that the Helmholtz equation (2.2) remains satisfied and no divergency occurs if $|z|$ tends to infinity. For the reflected wave ($z \geq 0$) we get

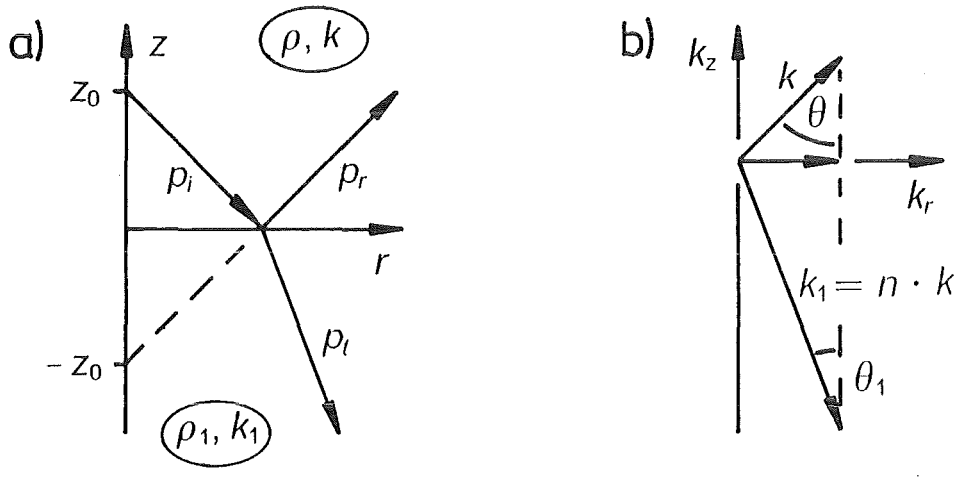

Fig.4: Our geometry (a) and description (b) of the angles θ for reflection and θ_1 for transmission in coordinates of wave numbers k. The harmonic point source is at $(r,z) = (0, z_0)$. $\sqrt{k^2 - k_r^2} \;=\; k \cos\theta$, $\sqrt{n^2k^2 - k_r^2} \;=\; nk \cos\theta_1$.

$$V(k, k_r) = \frac{m\sqrt{k^2 - k_r^2} - \sqrt{n^2k^2 - k_r^2}}{m\sqrt{k^2 - k_r^2} + \sqrt{n^2k^2 - k_r^2}} , \tag{3.7}$$

$$p_r(r,z) = i\int_0^\infty \frac{k_r dk_r}{\sqrt{k^2 - k_r^2}} J_0(k_r r)\, V(k, k_r) e^{(i\sqrt{k^2 - k_r^2}\,(z_0 + z))} , \tag{3.8}$$

and for the transmitted wave ($z \leq 0$)

$$W(k, k_r) = \frac{2m\sqrt{k^2 - k_r^2}}{m\sqrt{k^2 - k_r^2} + \sqrt{n^2k^2 - k_r^2}} , \tag{3.9}$$

$$p_t(r,z) = i\int_0^\infty \frac{k_r dk_r}{\sqrt{k^2 - k_r^2}} J_0(k_r r)\, W(k, k_r) e^{(i(\sqrt{k^2 - k_r^2}\, z_0 - \sqrt{n^2k^2 - k_r^2}\, z))} . \tag{3.10}$$

3.2 *Real expressions for the Sommerfeld integrals*

For numerical calculations the Sommerfeld forms (3.8) and (3.10) are not well suited due to irregularities at k_r near k. Here a simple coordinate transformation will help. To save CPU-time, real expressions with reduced variables are desirable in addition. It will turn out that for p_i three real integrals have to be evaluated. For p_r and p_t there are five integrals each; the forms of which depend on the sign of the quantity n - 1 . We will briefly describe the different steps and then give directly the relevant integrals and functions.

3.2.1 Transformation of k-coordinates

The Sommerfeld integrals are decomposed into two parts:

1. For the homogeneous component $0 \leq k_r \leq k$ the quantity $\kappa = \sqrt{k^2 - k_r^2}$ is real. κ is used as a new variable, and the substitution of $-d\kappa$ for $k_r dk_r / \sqrt{k^2 - k_r^2}$ eliminates the irregularity at $k_r = k$ or $\kappa = 0$.

2. For the inhomogeneous component $k_r > k$ the expression $\sqrt{k^2 - k_r^2}$ is purely imaginary. Here we use as new variable $\kappa' = i\sqrt{k_r^2 - k^2}$ and $d\kappa'$ replaces $ik_r dk_r / \sqrt{k^2 - k_r^2}$.

3.2.2 Reduced variables and notations

The scalar wave number k in the source medium is chosen as scale factor:

$$R = kr \quad , \quad Z = kz \quad , \quad Z0 = kz_0 \quad , \tag{3.10a, b, c}$$

$$K = \frac{\kappa}{k} \quad or \quad \frac{\kappa'}{k} \quad , \tag{3.10d}$$

$$PI = \frac{p_i}{k} \quad , \qquad PR = \frac{p_r}{k} \quad , \qquad PT = \frac{p_t}{k} \quad . \tag{3.10e, f, g}$$

Real and imaginary parts are marked by the two additional letters RE or IM (e.g. PTRE). Homogeneous and inhomogeneous components have the form XHOM and XINHOM, where X stands for I, R or T. In addition, we use capital letters (M and N) for the ratios m of densities and n of wave numbers or phase velocities, defined in Section 2.

3.2.3 The incident wave

Real and imaginary parts can directly be taken from (3.1):

$$PIRE = \frac{\cos(\sqrt{R^2 + (Z - Z0)^2})}{\sqrt{R^2 + (Z - Z0)^2}} \quad , \tag{3.11}$$

$$PIIM = \frac{\sin(\sqrt{R^2 + (Z - Z0)^2})}{\sqrt{R^2 + (Z - Z0)^2}} \quad . \tag{3.12}$$

To investigate the different constituents of the Sommerfeld integral, it is interesting to evaluate the homogeneous and inhomogeneous components separately. These are the relevant expressions:

$$IHOM = \int_0^1 dK\ F1I\ +\ i\int_0^1 dK\ F2I\ =\ PIHRE\ +\ i\,PIHIM \tag{3.13}$$

with

$$F1I = -J_0(\sqrt{1-K^2}\,R)\sin(K|Z-Z0|)\ , \tag{3.14}$$

$$F2I = +J_0(\sqrt{1-K^2}\,R)\cos(K|Z-Z0|)\ . \tag{3.15}$$

The inhomogeneous component is described by one real integral only:

$$IINHOM = \int_0^\infty dK\ F3I\ =\ PIINHOM \tag{3.16}$$

with

$$F3I = +J_0(\sqrt{1+K^2}\,R)e^{(-K|Z-Z0|)}\ . \tag{3.17}$$

Equations (3.11) and (3.12) then can be expressed by

$$PIRE\ =\ PIHRE + PIINHOM\ , \tag{3.18}$$

$$PIIM\ =\ PIHIM\ . \tag{3.19}$$

3.2.4 The reflected and transmitted waves for n > 1

The real and imaginary parts of the homogeneous components result from the integration of one real function for PR and PT each. The inhomogeneous components decompose into two sections ($0 < K\ < \sqrt{N^2-1}$ and $K > \sqrt{N^2-1}$) and three real functions are needed.

For the ***reflected wave PR*** ($z \geq 0$) we get

$$RHOM = \int_0^1 dK\ F1R\ +\ i\int_0^1 dK\ F2R\ =\ PRHRE + i\,PRHIM\ , \tag{3.20}$$

$$RINHOM = \int_0^{\sqrt{N^2-1}} dK\,(F4R \;+\; i\,F5R) \;+ \int_{\sqrt{N^2-1}}^{\infty} dK\,F3R$$

$$= (PRIRE1 + i\,PRIIM) \;+\; PRIRE2 \tag{3.21}$$

with

$$F1R \;=\; -J_0(R\sqrt{1-K^2})\,\sin(K(Z+Z0))\,\frac{MK - \sqrt{K^2+(N^2-1)}}{MK + \sqrt{K^2+(N^2-1)}}\;, \tag{3.22}$$

$$F2R \;=\; +J_0(R\sqrt{1-K^2})\,\cos(K(Z+Z0))\,\frac{MK - \sqrt{K^2+(N^2-1)}}{MK + \sqrt{K^2+(N^2-1)}}\;, \tag{3.23}$$

$$F3R = +J_0(R\sqrt{1+K^2})\,e^{(-K(Z+Z0))}\;\frac{MK - \sqrt{K^2-(N^2-1)}}{MK + \sqrt{K^2-(N^2-1)}}\;, \tag{3.24}$$

$$F4R = +J_0(R\sqrt{1+K^2})\,e^{(-K(Z+Z0))}\;\frac{(M^2+1)K^2 - (N^2-1)}{(M^2-1)K^2 + (N^2-1)}\;, \tag{3.25}$$

$$F5R = +J_0(R\sqrt{1+K^2})\,e^{(-K(Z+Z0))}\;\frac{2MK\sqrt{(N^2-1)-K^2}}{(M^2-1)K^2 + (N^2-1)}\;. \tag{3.26}$$

The final results for PR are obtained by combining the various contributions:

$$PRRE \;=\; PRHRE \;+\; PRIRE1 \;+\; PRIRE2 \tag{3.27}$$

$$PRIM \;=\; PRHIM \;+\; PRIIM \tag{3.28}$$

For the ***transmitted wave PT*** ($z \leq 0$) we get

$$THOM = \int_0^1 dK\, F1T \;+\; i\int_0^1 dK\, F2T \;=\; PTHRE + i\,PTHIM \tag{3.29}$$

$$TINHOM = \int_0^{\sqrt{N^2-1}} dK\,(F4T \;+\; i\,F5T) \;+\int_{\sqrt{N^2-1}}^{\infty} dK\, F3T$$

$$= (PTIRE1 + i\,PTIIM) \;+\; PTIRE2 \tag{3.30}$$

with

$$F1T = -J_0(R\sqrt{1-K^2})\sin(KZ0 - Z\sqrt{K^2+(N^2-1)})\frac{2MK}{MK+\sqrt{K^2+(N^2-1)}}\;, \tag{3.31}$$

$$F2T = +J_0(R\sqrt{1-K^2})\cos(KZ0 - Z\sqrt{K^2+(N^2-1)})\frac{2MK}{MK+\sqrt{K^2+(N^2-1)}}\;, \tag{3.32}$$

$$F3T = +J_0(R\sqrt{1+K^2})e^{(-KZ0+\sqrt{K^2-(N^2-1)}\,Z)}\frac{2MK}{MK+\sqrt{K^2-(N^2-1)}}\;, \tag{3.33}$$

$$F4T = +J_0(R\sqrt{1+K^2})e^{-KZ0}2MK$$

$$\cdot\;\frac{MK\cos(Z\sqrt{N^2-1-K^2})+\sqrt{N^2-1-K^2}\;\sin(Z\sqrt{N^2-1-K^2})}{(M^2-1)K^2+(N^2-1)}\;, \tag{3.34}$$

$$F5T = +J_0(R\sqrt{1+K^2})e^{-KZ0}2MK$$

$$\cdot\;\frac{\sqrt{N^2-1-K^2}\;\cos(Z\sqrt{N^2-1-K^2})-MK\sin(Z\sqrt{N^2-1-K^2})}{(M^2-1)K^2+(N^2-1)}\;. \tag{3.35}$$

The final results for PT are obtained by combining the various contributions:

$$PTRE \;=\; PTHRE \;+\; PTIRE1 \;+\; PTIRE2\;, \tag{3.36}$$

$$PTIM = PTHIM + PTIIM \ . \tag{3.37}$$

3.2.5 The reflected and transmitted waves for n < 1

The real and imaginary parts of the homogeneous components result from the integration of four real functions for PR and PT. The inhomogeneous component stems from only one real function for each wave field.

For the ***reflected wave PR*** ($z \geq 0$) we get

$$RHOM = \int_0^{\sqrt{N^2-1}} dK(F1R + iF2R) + \int_{\sqrt{N^2-1}}^{1} dK(F3R + iF4R) =$$

$$= (PRHRE1 + i\,PRHIM1) + (PRHRE2 + i\,PRHIM2) \ , \tag{3.38}$$

$$RINHOM = \int_0^{\infty} dKF5R = PRIRE \tag{3.39}$$

with

$$F1R = \frac{+ J_0(R\sqrt{1-K^2})}{(M^2-1)K^2 + (1-N^2)}$$

$$\cdot\ (2MK\sqrt{1-N^2-K^2}\ \cos(K(Z+Z0)) - ((M^2+1)K^2 - (1-N^2))\sin(K(Z+Z0))) \ , \tag{3.40}$$

$$F2R = \frac{+ J_0(R\sqrt{1-K^2})}{(M^2-1)K^2 + (1-N^2)}$$

$$\cdot\ (2MK\sqrt{(1-N^2)-K^2}\ \sin(K(Z+Z0)) + ((M^2+1)K^2 - (1-N^2))\cos(K(Z+Z0))) \ , \tag{3.41}$$

$$F3R = -J_0(R\sqrt{1-K^2})\sin(K(Z+Z0))\frac{MK - \sqrt{K^2-(1-N^2)}}{MK + \sqrt{K^2-(1-N^2)}} \ , \tag{3.42}$$

$$F4R = +J_0(R\sqrt{1-K^2})\cos(K(Z+Z0))\frac{MK-\sqrt{K^2-(1-N^2)}}{MK+\sqrt{K^2-(1-N^2)}} , \tag{3.43}$$

$$F5R = +J_0(R\sqrt{1+K^2})e^{(-K(Z+Z0))}\frac{MK-\sqrt{K^2-(1-N^2)}}{MK+\sqrt{K^2-(1-N^2)}} . \tag{3.44}$$

The final results for PR are obtained by combining the various contributions:

$$PRRE = PRHRE1 + PRHRE2 + PRIRE , \tag{3.45}$$

$$PRIM = PRHIM1 + PRHIM2 . \tag{3.46}$$

For the ***transmitted wave PT*** ($z \leq 0$) we get

$$THOM = \int_0^{\sqrt{1-N^2}} dK(F1T + iF2T) + \int_{\sqrt{1-N^2}}^{1} dK(F3T + iF4T)$$

$$= (PTHRE1 + i\,PTHIM1) + (PTHRE2 + i\,PTHIM2) , \tag{3.47}$$

$$TINHOM = \int_0^{\infty} dKF5T = PTIRE \tag{3.48}$$

with

$$F1T = +J_0(R\sqrt{1-K^2})e^{(Z\sqrt{(1-N^2)-K^2})}2MK$$

$$\cdot \frac{\sqrt{(1-N^2)-K^2}\cos(KZ0) - MK\sin(KZ0)}{(M^2-1)K^2+(1-N^2)} , \tag{3.49}$$

$$F2T = +J_0(R\sqrt{1-K^2})e^{(Z\sqrt{(1-N^2)-K^2})}2MK$$

$$\cdot \frac{\sqrt{(1-N^2)-K^2}\sin(KZ0) + MK\cos(KZ0)}{(M^2-1)K^2+(1-N^2)} , \tag{3.50}$$

$$F3T = -J_0(R\sqrt{1-K^2})\sin(KZ0 - Z\sqrt{K^2-(1-N^2)})\frac{2MK}{MK+\sqrt{K^2-(1-N^2)}}\ , \quad (3.51)$$

$$F4T = +J_0(R\sqrt{1-K^2})\cos(KZ0 - Z\sqrt{K^2-(1-N^2)})\frac{2MK}{MK+\sqrt{K^2-(1-N^2)}}\ , \quad (3.52)$$

$$F5T = +J_0(R\sqrt{1+K^2})e^{(-KZ0+Z\sqrt{K^2+(1-N^2)})}\frac{2MK}{MK+\sqrt{K^2+(1-N^2)}}\ . \quad (3.53)$$

The final results for PT are obtained by combining the various contributions:

$$PTRE = PTHRE1 + PTHRE2 + PTIRE\ , \quad (3.54)$$

$$PTIM = PTHIM1 + PTHIM2\ . \quad (3.55)$$

4. The Optical Coordinate System

Optical coordinates are the proper ones for the ray tube approximation decribed in Section 5. The optical coordinates are (see Fig. 5):

- r_0 , the radius of intersection with the refracting interface at z = 0 of a geometrical ray from the source at $Q = (0, z_0)$ to an arbitrary point X = (r,z).
- s, the optical path or eikonal between Q and X, and
- φ , the usual azimuthal angle around the z-axis.

In agreement with the Fermat principle, the optical coordinate system is orthogonal, and the differential operators can be derived in the usual way. The relations between optical and cylindrical coordinates for the reflected wave are different from those for the transmitted wave. This section will be subdivided accordingly. The azimuthal angle φ, which

has the same meaning in both coordinate systems, will be mentioned only when needed. Throughout this section we will use the abbreviations (not to be confused with the densities):

$$\rho = \sqrt{r_0^2 + z_0^2} \quad , \tag{4.1}$$

$$\rho_1 = \sqrt{(n^2-1)r_0^2 + n^2 z_0^2} \quad . \tag{4.2}$$

4.1 *Transformations between cylindrical and optical coordinates*

4.1.1 For the reflected wave

For this wave the relative refractive index is n = 1 and $z \geq 0$. The relations between (r,z) and (r_0,s) can directly be read from Fig. 5a:

$$r_0 = \frac{rz_0}{z + z_0} \quad , \tag{4.3}$$

$$s = \frac{\rho(z + z_0)}{z_0} \quad , \tag{4.4}$$

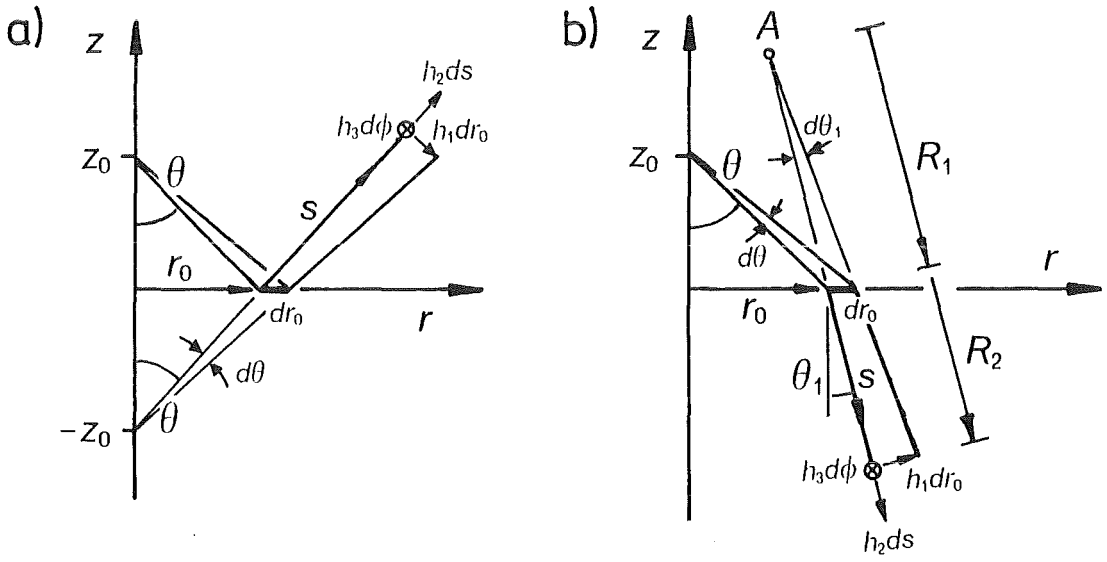

Fig.5: For derivation of the scale factors h_i of optical coordinates r_0, s, ϕ for the reflected wave (a) and for the transmitted wave (b).

$$r = \frac{r_0 s}{\rho} \quad , \tag{4.5}$$

$$z = \frac{z_0(s-\rho)}{\rho} \quad . \tag{4.6}$$

4.1.2 For the transmitted wave

For this wave $n \neq 1$ and $z \leq 0$ and the identity

$$\cos\theta = \frac{z_0}{\rho} \tag{4.7}$$

together with the Snellius relations (2.12) leads to

$$\cos\theta_1 = \frac{\rho_1}{n\rho} \quad . \tag{4.8}$$

Supposing $r_0 = r_0(r,z)$ to be known, the following three expressions are quickly derived from Fig. 5b:

$$s = \rho + n\sqrt{(r-r_0)^2 + z^2} \quad , \tag{4.9}$$

$$r = r_0 + \frac{1}{n}(s-\rho)\sin\theta = r_0(1 + \frac{s-\rho}{n^2\rho}) \quad , \tag{4.10}$$

$$z = -\frac{1}{n}(s-\rho)\cos\theta_1 = -\rho_1\frac{s-\rho}{n^2\rho} \quad . \tag{4.11}$$

It is quite a long way to derive r_0 from r and z for the transmitted wave. It is done by solving the fourth order equation

$${r_0}^4 - 2r{r_0}^2 + (r^2 + \frac{n^2{z_0}^2}{n^2-1} - \frac{z^2}{n^2-1}){r_0}^2 - \frac{2n^2{z_0}^2 r_0 r}{n^2-1} + \frac{n^2{z_0}^2}{n^2-1}r^2 = 0 \tag{4.12}$$

in r_0 which results from $n\sin\theta_1 = \sin\theta$ after two squarings. One gets up to four real values for r_0 (see e.g. [10] ,p 183 ff), two of which may be relevant in our case. In the

following expressions upper signs are valid for the case n > 1, lower signs for n < 1 . One starts by calculating the quantities

$$\Delta = \frac{n^2 z_0^{\,2} - z^2}{n^2 - 1} \quad , \tag{4.13}$$

$$P = \frac{-1}{3}(r^2 + \Delta^2) \quad , \tag{4.14}$$

$$Q = -2\left(\left(\frac{(r^2 + \Delta)}{3}\right)^3 + 2\left(\frac{nz_0 rz}{n^2 - 1}\right)^2\right) \quad , \tag{4.15}$$

$$W = \frac{1}{3}(r^2 - 2\Delta) \quad , \tag{4.16}$$

$$D = \left(\frac{1}{3}(r^2 + \Delta)\right)^3 + \left(\frac{nz_0 rz}{n^2 - 1}\right)^2 \quad , \tag{4.17}$$

$$R = sgn(Q)\sqrt{\frac{|P|}{3}} \quad . \tag{4.18}$$

Special precautions must be taken for the case R = 0. If the determinant D is positive, then

$$\Phi = \frac{1}{3}\ln\left(\frac{Q}{2R^3} + \sqrt{\left(\frac{Q}{2R^3}\right)^2 - 1}\right) \quad , \tag{4.19}$$

$$U = R\cosh\Phi \quad , \tag{4.20}$$

$$V = \sqrt{3}\, R \sinh\Phi \quad , \tag{4.21}$$

$$\varphi_1 = \frac{1}{2}\arccos\frac{W + U}{\sqrt{(W + U)^2 + V^2}} \quad , \tag{4.22}$$

$$UV = 2((W + U)^2 + V^2)^{\frac{1}{4}} \cos\varphi_1 \tag{4.23}$$

are calculated. Then r_0 is given by

$$r_0 = \frac{1}{2}(r \pm \{\sqrt{W - 2U} - UV\}) \quad . \tag{4.24}$$

If D is smaller than or equal to zero, then

$$\varphi = \frac{1}{3} \arccos\left(\frac{Q}{2R^3}\right) , \tag{4.25}$$

$$U = R\cos\varphi , \tag{4.26}$$

$$V = \sqrt{3}\, R \sin\varphi \tag{4.27}$$

are calculated, and r_0 is given by

$$r_0 = \frac{1}{2}\left(r \pm \left\{\sqrt{W-2U} - \sqrt{W+U+V} - \sqrt{W+U-V}\right\}\right) . \tag{4.28}$$

Under very special conditions, this value is outside the physical range $0 \leq r_0 \leq r$. In this case, for $D \leq 0$, use

$$r_0 = \frac{1}{2}\left(r \mp \left\{\sqrt{W-2U} + \sqrt{W+U-V} - \sqrt{W+U+V}\right\}\right) . \tag{4.29}$$

Before starting the determination of r_0, the following special cases are interrogated:

$$\text{if } r = 0: \qquad r_0 = 0 , \tag{4.30}$$

$$\text{if } z = 0 \text{ and } n > 1: \qquad r_0 = r , \tag{4.31}$$

$$\text{if } z = 0 \text{ and } n < 1: \qquad r_0 = min\left(r, \frac{nz_0}{\sqrt{1-n^2}}\right) . \tag{4.32}$$

4.2 *Differential operators in optical coordinates*

Differential operators for curvilinear orthogonal coordinates are expressed in terms of scale factors h_i (see e.g. [11] , p 41 ff). These are obtained by expressing a line element $ds = \sqrt{dx^2 + dy^2 + dz^2}$ (x,y,z = Cartesian coordinates) by elements of the curvilinear coordinates. For optical coordinates, this leads to

$$ds^2 = h_1^2 dr_0^2 + h_2^2 ds^2 + h_3^2 d\varphi^2 . \tag{4.33}$$

If the scale factors are known, the usual differential operators are given by:

$$\vec{\nabla}\Phi = \left(\frac{1}{h_1}\frac{\partial\Phi}{\partial r_0}, \frac{1}{h_2}\frac{\partial\Phi}{\partial s}, \frac{1}{h_3}\frac{\partial\Phi}{\partial\varphi}\right) , \tag{4.34}$$

$$\vec{\nabla}\cdot\vec{A} = \frac{1}{h_1h_2h_3}\left(\frac{\partial}{\partial r_0}(h_2h_3A_1) + \frac{\partial}{\partial s}(h_1h_3A_2) + \frac{\partial}{\partial\varphi}\left(\frac{h_1h_2}{h_3}A_3\right)\right) , \tag{4.35}$$

$$\Delta\Phi = \frac{1}{h_1h_2h_3}\left(\frac{\partial}{\partial r_0}\frac{h_2h_3}{h_1}\frac{\partial\Phi}{\partial r_0} + \frac{\partial}{\partial s}\frac{h_1h_3}{h_2}\frac{\partial\Phi}{\partial s} + \frac{\partial}{\partial\varphi}\frac{h_1h_2}{h_3}\frac{\partial\Phi}{\partial\varphi}\right) . \tag{4.36}$$

The scale factors and the differential operators have different shapes for the reflected and for the transmitted waves. In the following subsections we will give the scale factors and the Laplace operator only.

4.2.1 For the reflected wave

The scale factors are determined for the geometrical conditions shown in Fig. 5a. Using the relations (2.12), (4.7), and (4.8), one gets

$$h_1dr_0 = s\frac{dr_0\cos\theta}{\sqrt{r_0^2 + z_0^2}} = \frac{sz_0}{\rho^2}dr_0 , \tag{4.37}$$

$$h_2ds = ds , \tag{4.38}$$

$$h_3d\varphi = rd\varphi = \frac{r_0s}{\rho}d\varphi . \tag{4.39}$$

The Laplace operator (4.36) takes the form

$$\Delta = \frac{\rho^3}{r_0s^2z_0^2}\frac{\partial}{\partial r_0}\left(r_0\rho\frac{\partial}{\partial r_0}\right) + \frac{1}{s^2}\frac{\partial}{\partial s}\left(s^2\frac{\partial}{\partial s}\right) + \frac{\rho^2}{s^2r_0^2}\frac{\partial^2}{\partial\varphi^2} . \tag{4.40}$$

4.2.2 For the transmitted wave

The geometrical conditions are shown in Fig. 5b. To derive the first scale factor we must know the distance R_1 between the backward intersection A of two infinitesimally adjacent rays and the point of impact $(r,z) = (r_0,0)$ on the diffracting plane:

$$R_1 = \frac{\sqrt{r_0^2 + z_0^2}\, d\theta}{\cos\theta} \frac{\cos\theta_1}{d\theta_1} = \frac{\rho\rho_1^2}{nz_0^2} \quad . \tag{4.41}$$

The distance between A and a point of interest, defined by its optical coordinates, is

$$R_2 = R_1 + \frac{1}{n}(s - \sqrt{r_0^2 + z_0^2}) = \frac{1}{n}(s + (n^2 - 1)\frac{\rho^3}{z_0^2}) \quad . \tag{4.42}$$

With these auxiliary quantities we get

$$h_1 dr_0 = \frac{R_2 \cos\theta_1}{R_1} dr_0 = \frac{z_0^2}{n\rho^2\rho_1}(s + (n^2 - 1)\frac{\rho^3}{z_0^2})dr_0 \quad , \tag{4.43}$$

$$h_2 ds = \frac{ds}{n} \quad , \tag{4.44}$$

$$h_3 d\varphi = r d\varphi = \frac{r_0}{n^2\rho}(s + (n^2 - 1)\rho)d\varphi \quad . \tag{4.45}$$

The Laplace operator (4.36) can now be written as

$$\Delta = \frac{n^2 R_1 \rho}{R_2 r \rho_1} \frac{\partial}{\partial r_0}\left(\frac{R_1 r \rho}{R_2 \rho_1}\frac{\partial}{\partial r_0}\right) + \frac{n^2}{R_2 r}\frac{\partial}{\partial s}\left(R_2 r \frac{\partial}{\partial s}\right) + \frac{1}{r^2}\frac{\partial^2}{\partial \varphi^2} \quad , \tag{4.46}$$

where R_1, R_2, r, ρ, ρ_1, are given by (4.41), (4.42), (4.10), (4.1) and (4.2), respectively.

4.3 The boundary conditions in optical coordinates

The diffracting plane $z = 0$ is described by

$$s = \rho \quad . \tag{4.47}$$

The ***kinematic boundary condition*** (2.11) can be written as

$$p_i(r_0, \rho) + p_r(r_0, \rho) = p_t(r_0, \rho) \quad . \tag{4.48}$$

For the ***dynamic boundary condition*** (2.14) we have to express the gradient $\partial/\partial z$ in z-direction by optical variables. It is easily shown that

for $p_i(r_0, s)$

$$\frac{\partial}{\partial z} = \frac{\sin\theta}{h_1}\frac{\partial}{\partial r_0} - \frac{\cos\theta}{h_2}\frac{\partial}{\partial s} = \frac{r_0\rho}{sz_0}\frac{\partial}{\partial r_0} - \frac{r_0}{\rho}\frac{\partial}{\partial s} \quad , \tag{4.49}$$

for $p_r(r_0, s)$

$$\frac{\partial}{\partial z} = -\frac{\sin\theta}{h_1}\frac{\partial}{\partial r_0} + \frac{\cos\theta}{h_2}\frac{\partial}{\partial s} = \frac{-r_0\rho}{sz_0}\frac{\partial}{\partial r_0} + \frac{r_0}{\rho}\frac{\partial}{\partial s} \quad , \tag{4.50}$$

for $p_t(r_0, s)$

$$\frac{\partial}{\partial z} = \frac{\cos\theta_1}{h_1}\frac{\partial}{\partial r_0} - \frac{\sin\theta_1}{h_2}\frac{\partial}{\partial s} = \frac{R_1 r_0}{R_2\rho_1}\frac{\partial}{\partial r_0} - \frac{\rho_1}{\rho}\frac{\partial}{\partial s} \quad . \tag{4.51}$$

At the boundary $s = \rho$, $R_1 = R_2$, and the dynamic boundary condition takes the form

$$\left(\frac{r_0}{z_0}\frac{\partial}{\partial r_0} - \frac{z_0}{\rho}\frac{\partial}{\partial s}\right)(p_i(r_0,s) - p_r(r_0, s))\Big|_{s=\rho} = \frac{1}{m}\left(\frac{r_0}{\rho_1}\frac{\partial}{\partial r_0} - \frac{\rho_1}{\rho}\frac{\partial}{\partial s}\right)p_t(r_0,s)\Big|_{s=\rho} . \tag{4.52}$$

Remember that m is the density ratio in Eq. (2.15).

5. The Ray Tube Approximation (RTA)

The RTA is used in geometrical optics (see e.g. [5] , p 109 ff). It is a good approximation if the wavelength is small with respect to geometrical dimensions. The following assumptions are made:

- Rays within the waves propagate perpendicularly to surfaces of constant eikonal or optical path.

- In optically homogeneous media the propagation is rectilinear.

- The diffraction at the interface between two homogeneous media can be described by the Fresnel coefficients for plane waves.

- The energy flux through surface elements, which are limited by the same rays (ray tube), is independent of the coordinate along the rays.

In this section we will restrict ourselves to the case n > 1. For n < 1 total reflection will occur if the radius r_0 of impact at z = 0 (see Fig. 5) is larger than the limiting radius

$$r_{0l} = z_0 \frac{n}{\sqrt{1-n^2}} \quad . \tag{5.1}$$

Then, inhomogeneous waves will penetrate into the diffracting medium which at $r_0 = r_{0l}$ will not be attenuated but extend to $z \to -\infty$. This causes irregularities which, in physics terms, make no sense. We conclude that the RTA is not suited to describe diffracton of spherical waves in the case n < 1.

From the assumptions of the RTA it follows that the phase of a spherical scalar harmonic wave is given by the optical path s and that the amplitude is inversely proportional to the square root of a tube cross section. Due to the use of Fresnel coefficients, the energy flux will be conserved at the interface (as described in Subsection 2.4), and the kinematical and dynamical boundary conditions (2.11) and (2.14) will be fulfilled. However, the Helmholtz equation (2.2) is violated in p_r and p_t .This can be shown by lengthy calculations in a general form. We demonstrate it numerically for the examples given in Subsection 6.3, Figs. 34 and 37.

5.1 The incident wave

The cross section of a ray tube is proportional to the square of the optical path s and thus

$$p_i(r_0,s) = \frac{e^{iks}}{s} \quad . \tag{5.2}$$

It is identical to (3.1) and fulfills the Helmholtz equation (2.2).

5.2 The reflected wave

From Fig. 5a it follows that the cross section of a ray tube behaves as for the incident wave. The reflection coefficient V (2.16) can be expressed by optical coordinates with the auxiliary quantities ρ, ρ_1 (see (4.7) and (4.8)), and we get

$$p_r(r_0, s) = \frac{mz_0 - \rho_1}{mz_0 + \rho_1} \frac{e^{iks}}{s} \quad . \tag{5.3}$$

5.3 The transmitted wave

From Fig. 5b it can be seen that the cross section $dF(r_0, s)$ of a ray tube, defined by $d\theta$ *and* $d\varphi$, is

$$dF(r_0, s) = R_2 d\theta_1 r d\varphi \quad . \tag{5.4}$$

At the interface we have

$$dF_0(r_0, s = \rho) = R_1 d\theta_1 r_0 d\varphi \quad . \tag{5.5}$$

Since $|p_t(r_0, s)| = \left(\frac{dF_0}{dF}\right)^{\frac{1}{2}} |p_t(r_0, s = \rho)|$ *we get*

$$p_t(r_0, s) = W \sqrt{\frac{r_0}{r} \frac{R_1}{R_2}} \frac{e^{iks}}{\rho} \quad . \tag{5.6}$$

R_1, R_2, r, and ρ are given in (4.41), (4.42), (4.10), and (4.1). W follows from (2.17) using (4.7) and (4.8):

$$W = \frac{2mz_0}{mz_0 + \rho_1} \tag{5.7}$$

with ρ_1 given in (4.2) .

6. Some Numerical Results

In this section examples are shown for wave fields obtained by the strict Sommerfeld method and from the ray tube approximation (RTA). We will call them here Sommerfeld and RTA waves. The following parameters have been chosen:

- Z0 = 3 in reduced units (see Eq.(3.10c)). This means that in all cases the point source is about half a wavelength above the refracting plane.

- N = 2 and N = 0.5. This means that examples are shown for diffraction from and into an acoustically thinner medium.

- M = 1 and $M = N^2$. This means that combinations of the relative refractive index N and the density ratio M are chosen which could be extended to describe the diffraction of spherical electromagnetic dipole waves (see Eq.(2.18)).

The wave fields are figured as two-dimensional plots in reduced cylindrical coordinates. In each case the real and imaginary parts were calculated in steps of 0.1 reduced unit for R = 0 to 20 and $|Z| = 0$ to 15. From these twice 151 x 201 = 60,702 primary data the quantities of interest were deduced using simple FORTRAN routines and plotted with the FORTRAN graphics subroutine library CA-DISSPLA (Display Integrated Software System and Plotting LAnguage [12]). For Sommerfeld waves the homogeneous and inhomogeneous components are figured in addition. The calculation of involved integrals in k-space is described in Subsection 6.1.

6.1 *The incident wave*

This wave was calculated analytically (Fig.6) and following the Sommerfeld integral formalism (Fig.7). The Sommerfeld wave is the sum of its homogeneous component (Fig.8) and its inhomogeneous component (Fig.9). It reproduces the circular structure of absolute value and phase angle sufficiently well. Only in Fig.7a, slight wiggles can be seen at $Z = Z0$ where the integrand (3.17) of the inhomogeneous component has no exponential damping factor, and therefore (3.16) converges very slowly.

The Sommerfeld waves shown in this section are obtained from trapezoidal integration in k-space. Finite integrals are calculated with up to 2,000 integration intervals. Infinite integrals were extended up to $k_{max} = 200$ with up to 16,000 integration intervals. It turned out that the quality of infinite integrals depends critically on the width of integration intervals, whereas an increase in k_{max} produced no improvement. Homogeneous components, as shown in Fig.8, exhibit points of zero absolute value with ambiguities in phase angle. Turning around these points changes the phase angle by 2π . DISSPLA generates in such cases lines of discontinuity. These lines were eliminated by hand. Only those branches are labeled which are essentially stable when the inhomogeneous component is added to form the complete Sommerfeld wave.

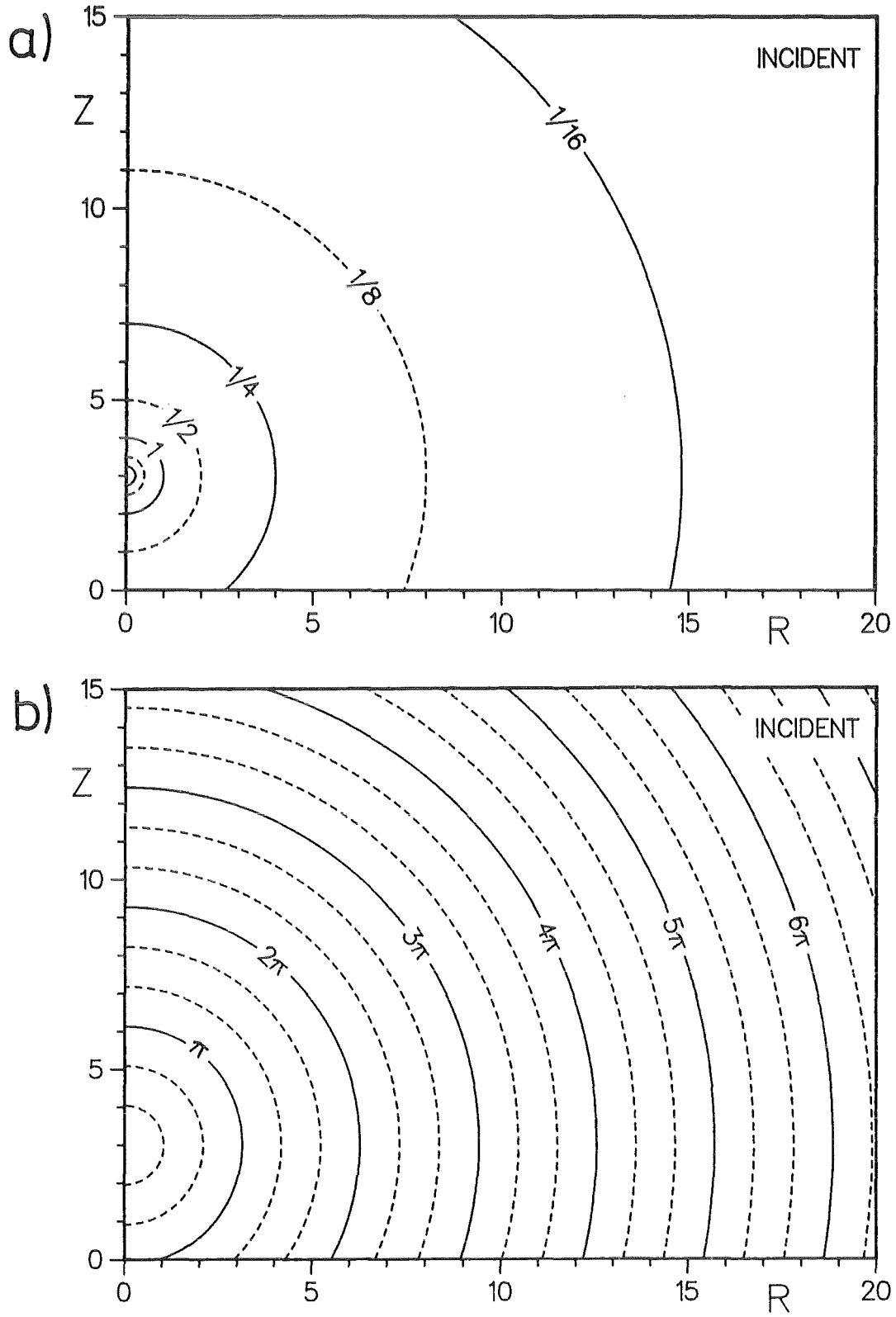

Fig.6: Absolute value (a) and phase angle (b) of the incident wave obtained from the analytical expressions (3.11) and (3.12). Their isolines will be used for comparison in subsequent figures.

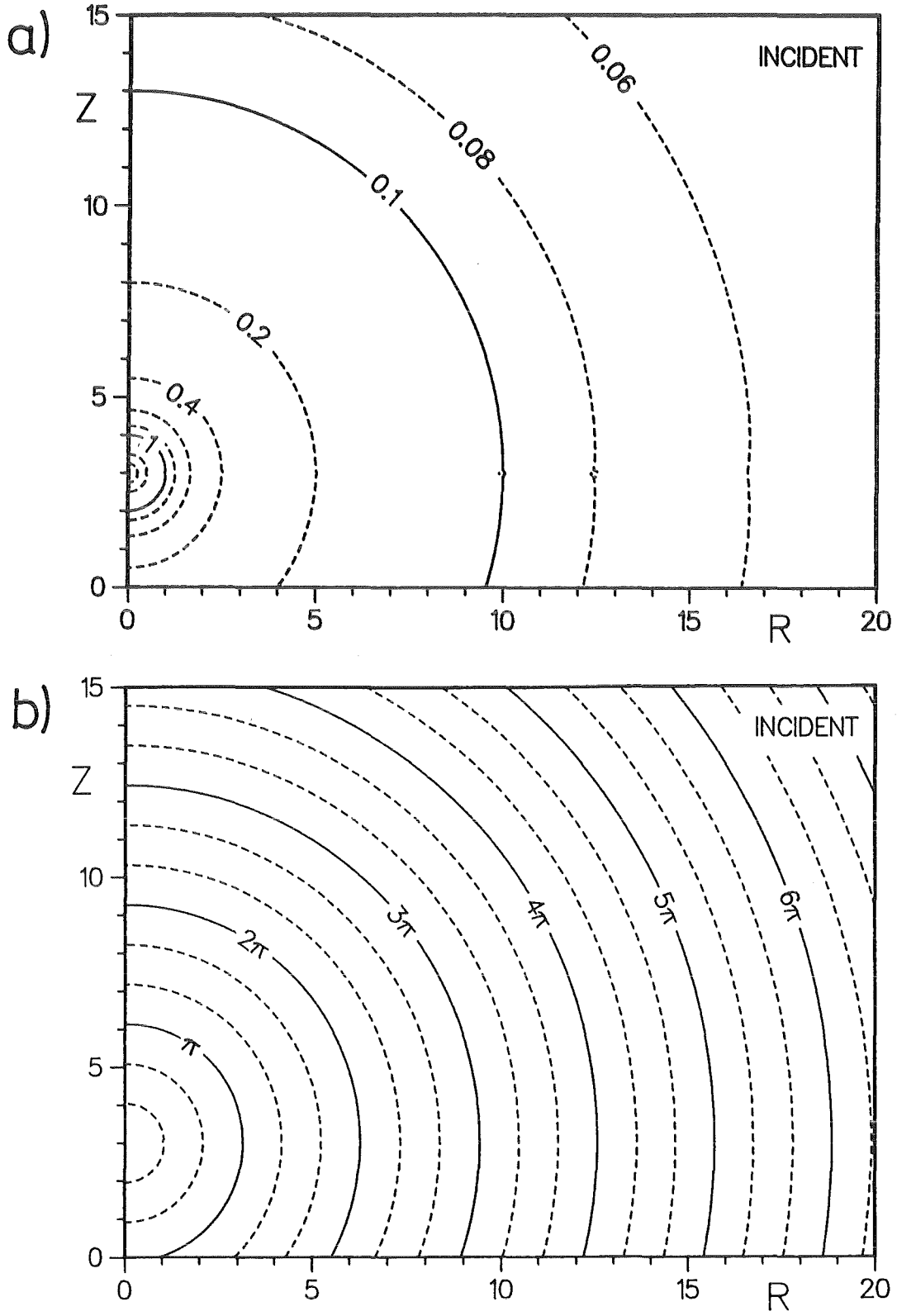

Fig.7: Absolute value (a) and phase angle (b) of the incident wave calculated following the Sommerfeld integral description, Eqs. (3.13) to (3.19).

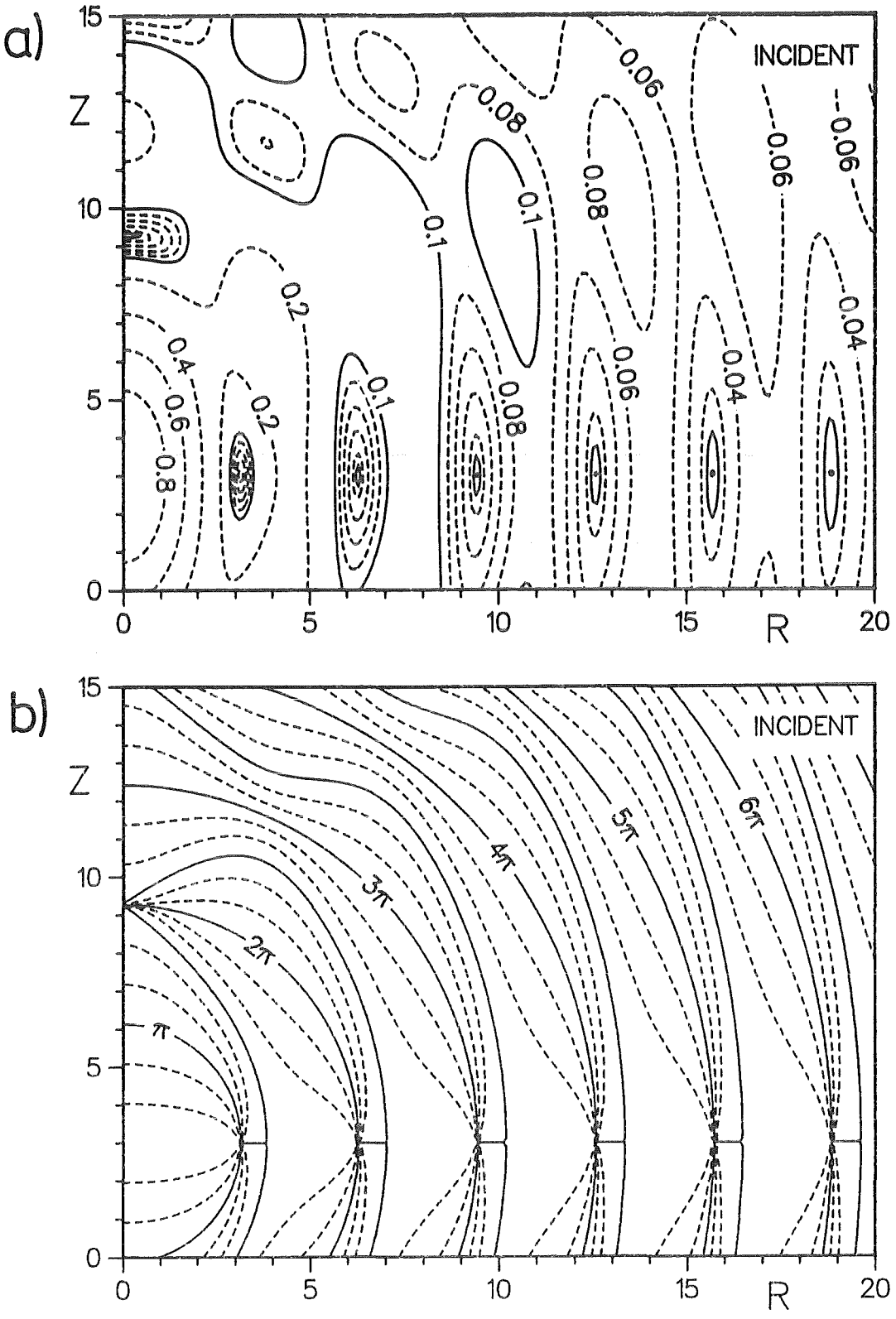

Fig.8: Absolute value (a) and phase angle (b) of homogeneous component of the incident wave as defined by Eqs. (3.13) to (3.15).

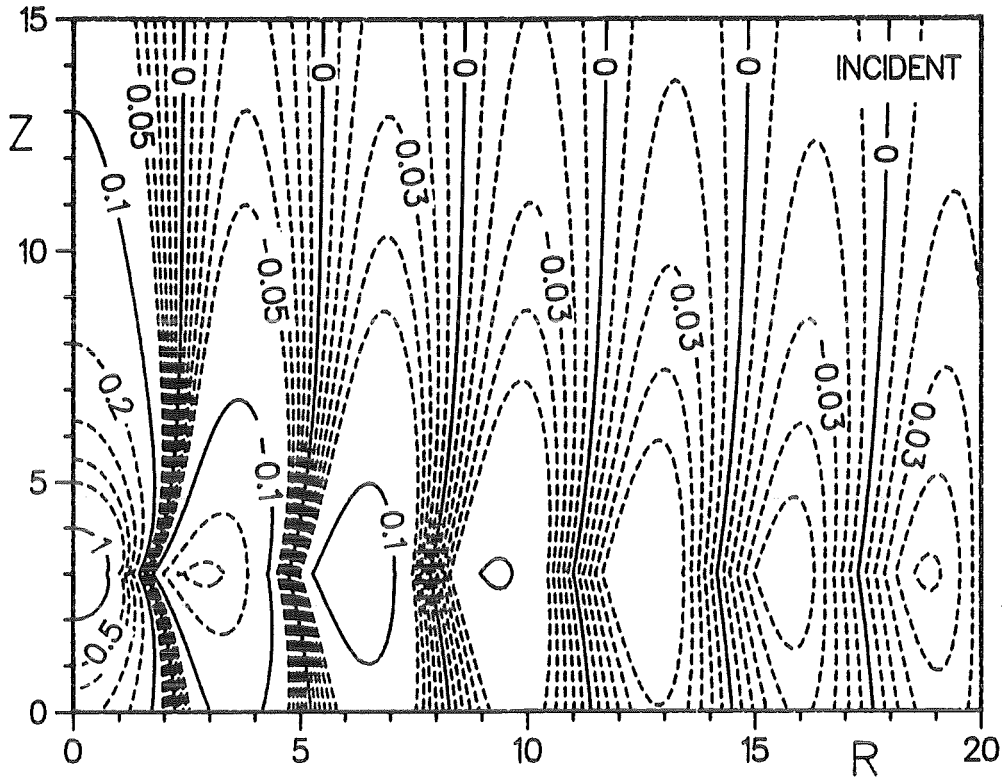

Fig.9: The inhomogeneous component of the incident wave as defined by Eqs. (3.16) to (3.19).

6.2 *Sommerfeld waves for reflection and transmission*

The reflected (PR) and transmitted (PT) Sommerfeld waves and their homogeneous and inhomogeneous components for the parameter combinations N = 2, 0.5 and M = 1, N^2 are shown in Figs.10 to 31. The inhomogeneous components are complex for N = 2 and real for N = 0.5 (see Eqs. (3.21), (3.30) and (3.39), (3.48)).

The case ***M = 1, N = 2*** (Figs.10 to 15) corresponds to Fig.3b for plane waves. The negative sign of the local reflection coefficient is expressed in Fig.11 by a shift of the PR phase with respect to PI at Z = 0 of about $-\pi$. The spurious irregularities of PT in Figs.10 and 11 could be suppressed by a greater computational effort than described in Subsection 6.1.

The case ***M = 4, N = 2*** (Figs.16 to 21) corresponds to Fig.3a for plane waves. A line through the relative minima of PR in Fig.16 describes roughly the angle θ of incidence in Fig.3a for which the reflection coefficient vanishes.

The case ***M = 1, N = 0.5*** (Figs.22 to 26) corresponds to Fig.3c for plane waves. The point of ambiguous phase angle near (R,Z) = (16,-2) in Figs.25 and 26 persists when the inhomogeneous component is added. Thus, the corresponding points in Figs.22 and 23 figure an interesting mechanism of absorption of phase excess in the acoustically thinner medium. We expect that such zero points of phase absorption appear periodically for R > 20.

The case ***M = 0.25, N = 0.5*** (Figs.27 to 31) corresponds to Fig.3d for plane waves. The point of phase absorption in PT for M = 1 (Figs.22 and 23) seems to be shifted in Figs.27 and 28 to the region Z > 0 which is outside the physical range of PT. It would be interesting to know how PT behaves in this case for R > 20.

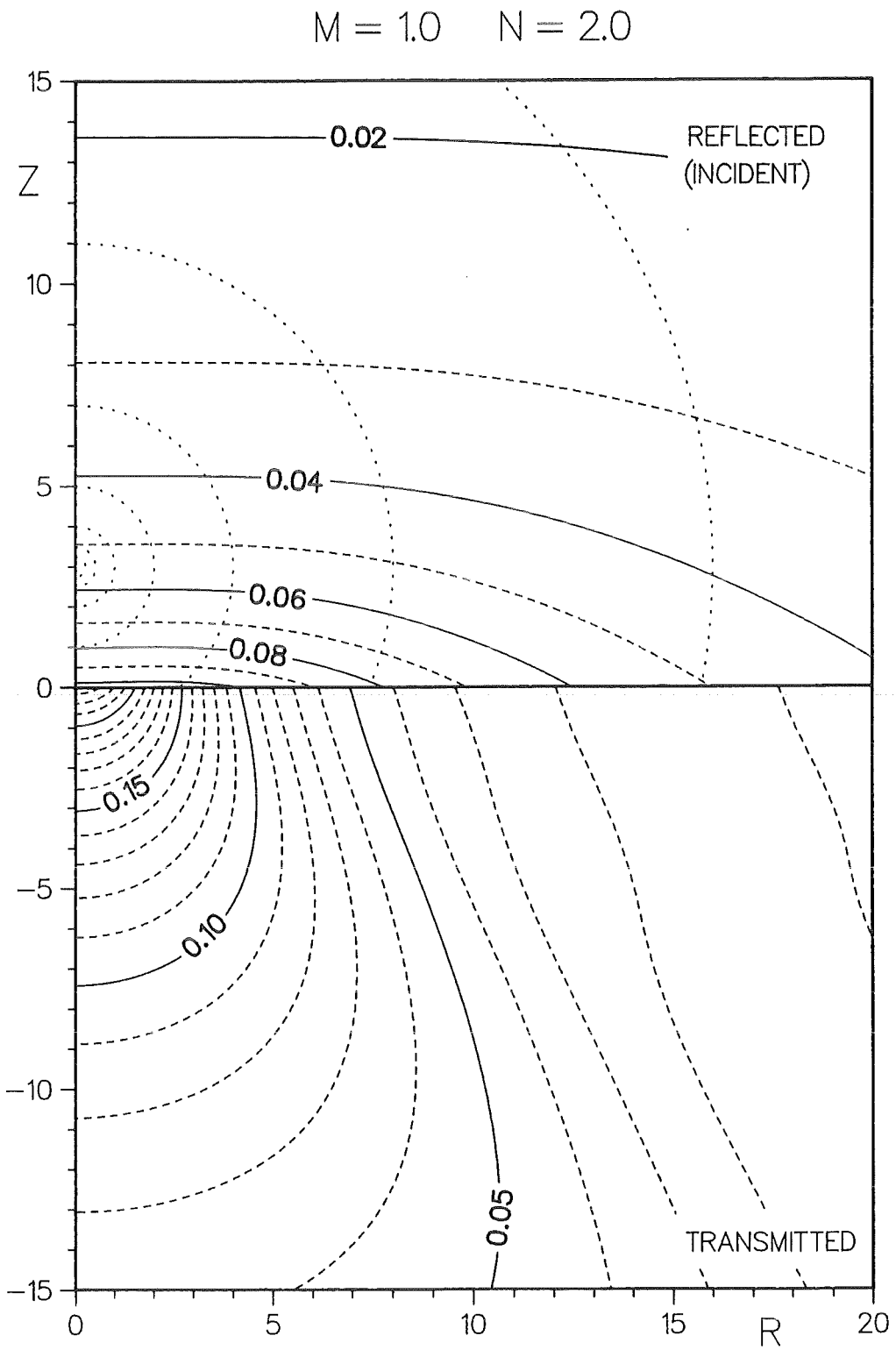

Fig.10:The absolute values of the reflected and transmitted Sommerfeld waves for the ratios M and N of densities and phase velocities given above. For labels of the indicated incident wave, see Fig.6a.

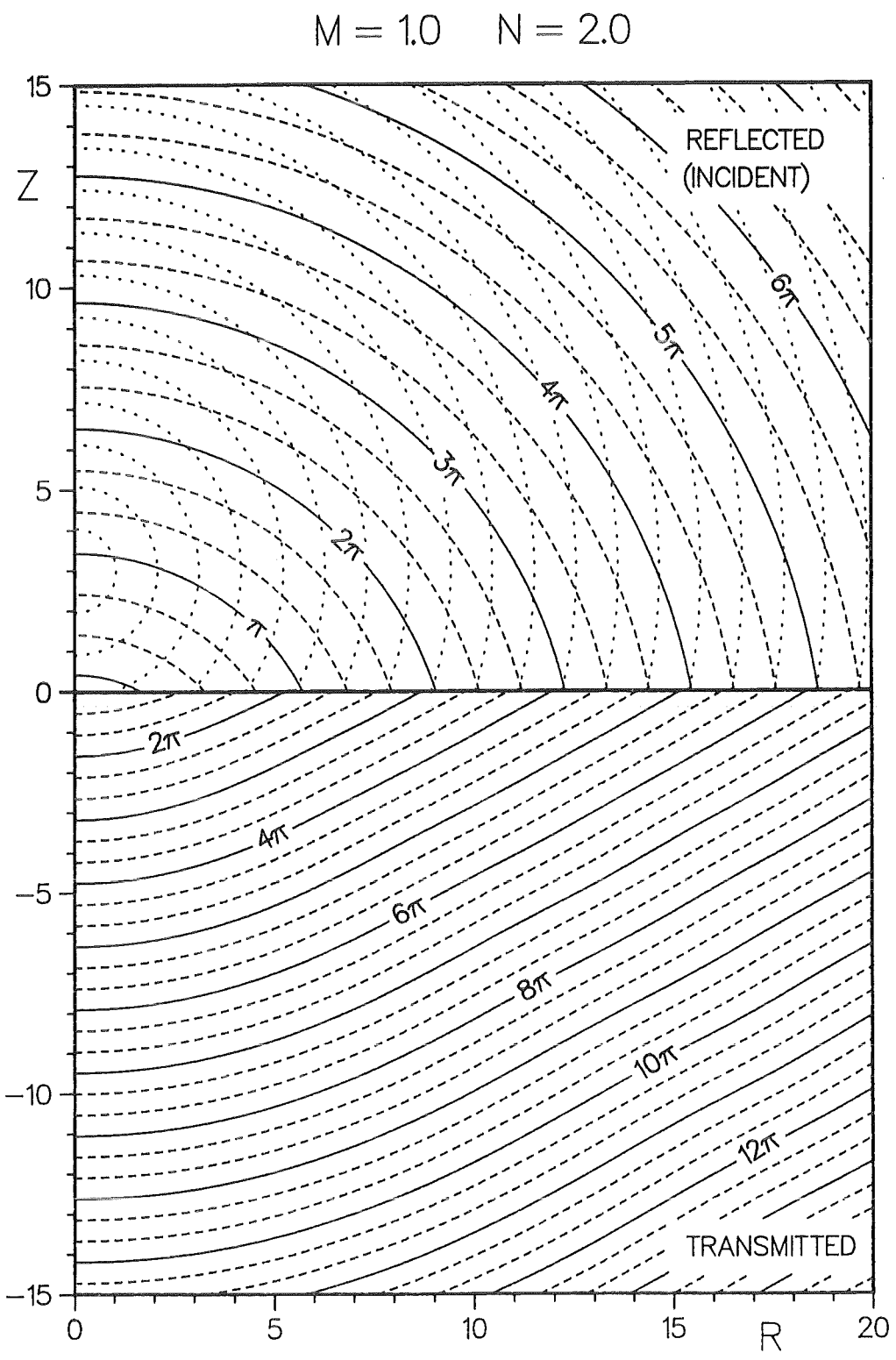

Fig.11: Phase angle of the reflected and transmitted Sommerfeld waves for the ratios M and N of densities and phase velocities given above. For labels of the indicated incident wave, see Fig.6b.

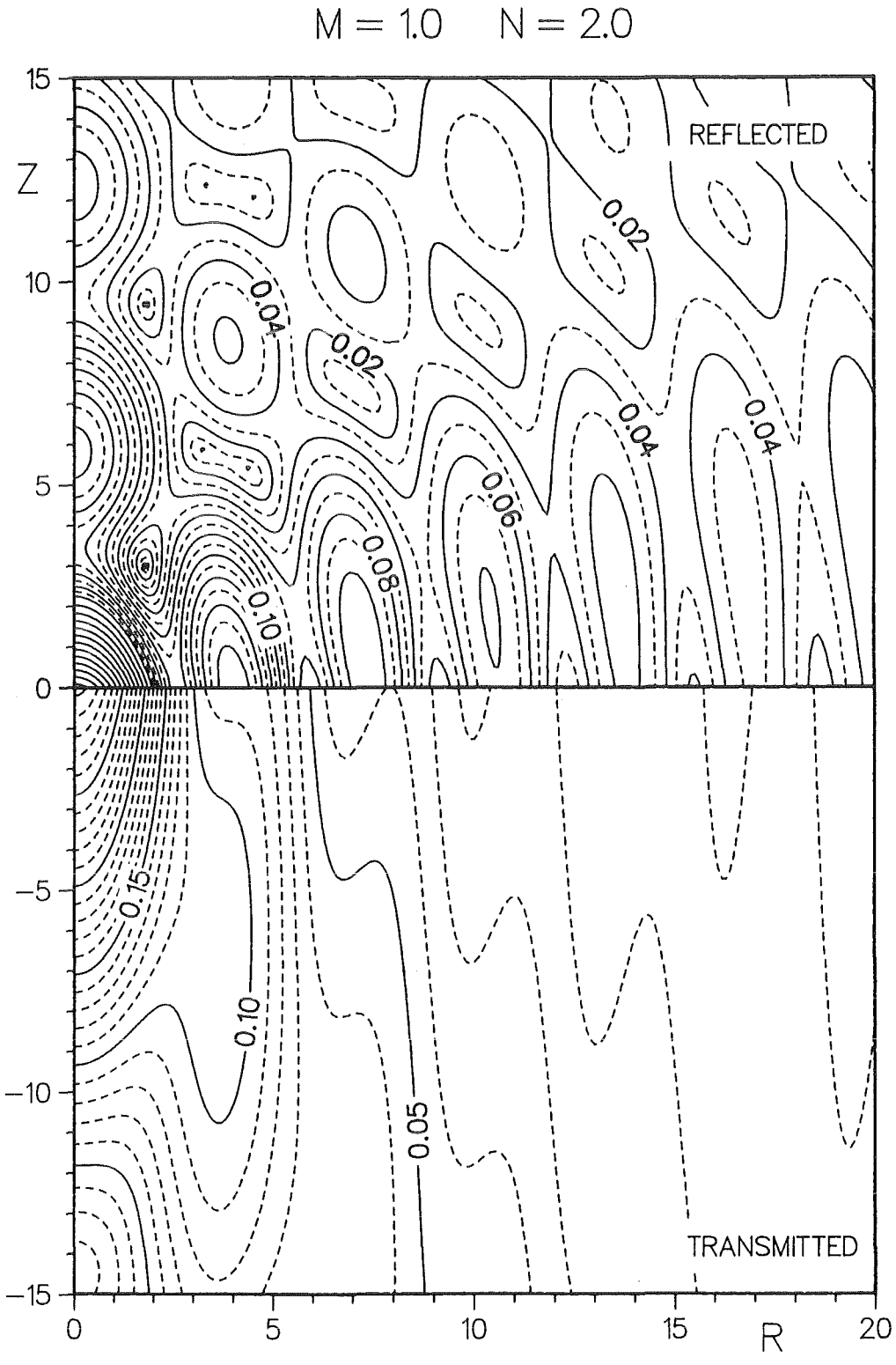

Fig.12: The absolute values of the homogeneous components of the Sommerfeld waves for the ratios M and N of densities and phase velocities given above.

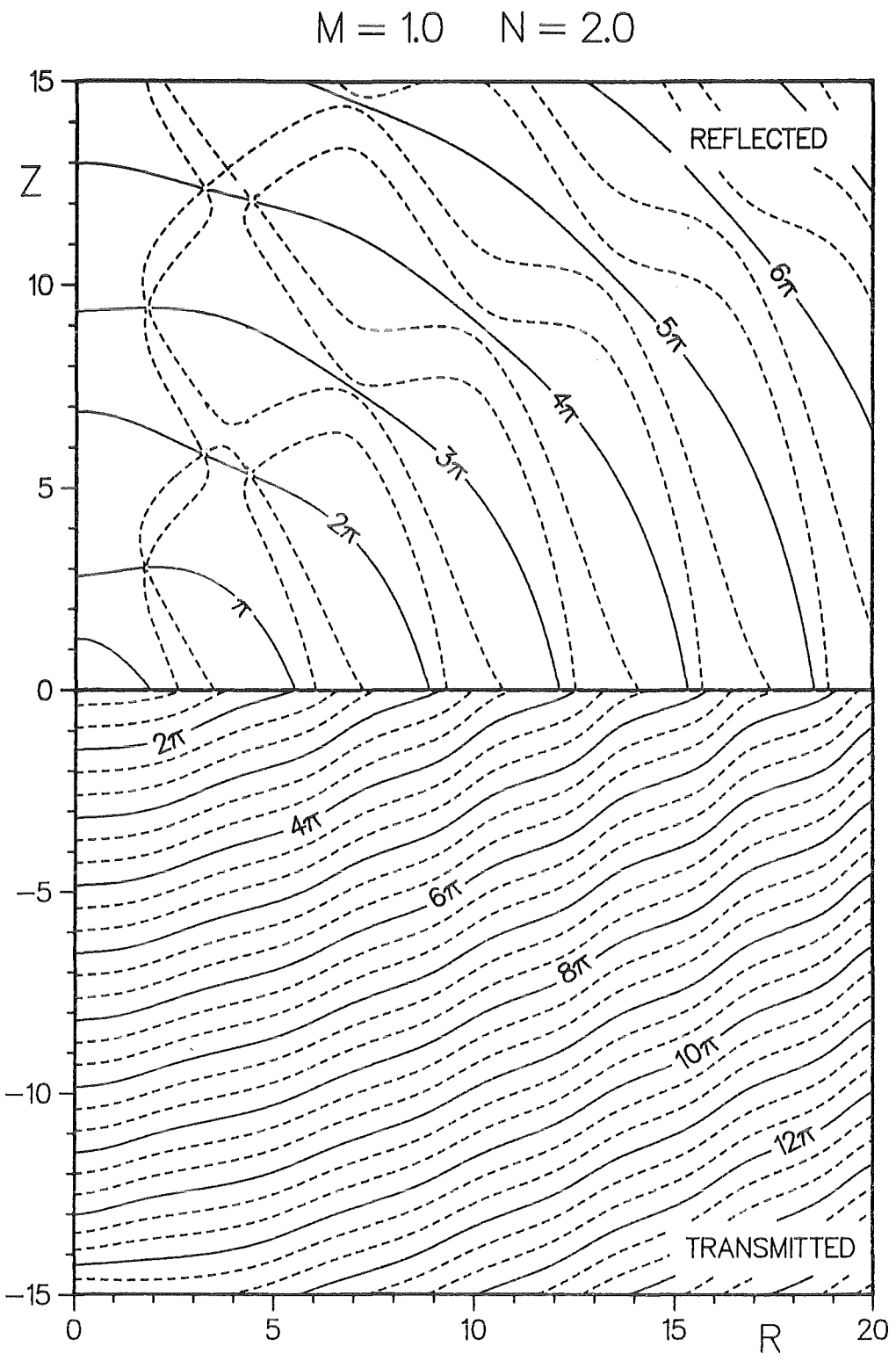

Fig.13: The phase angles of the homogeneous components of the Sommerfeld waves for the ratios M and N of densities and phase velocities given above.

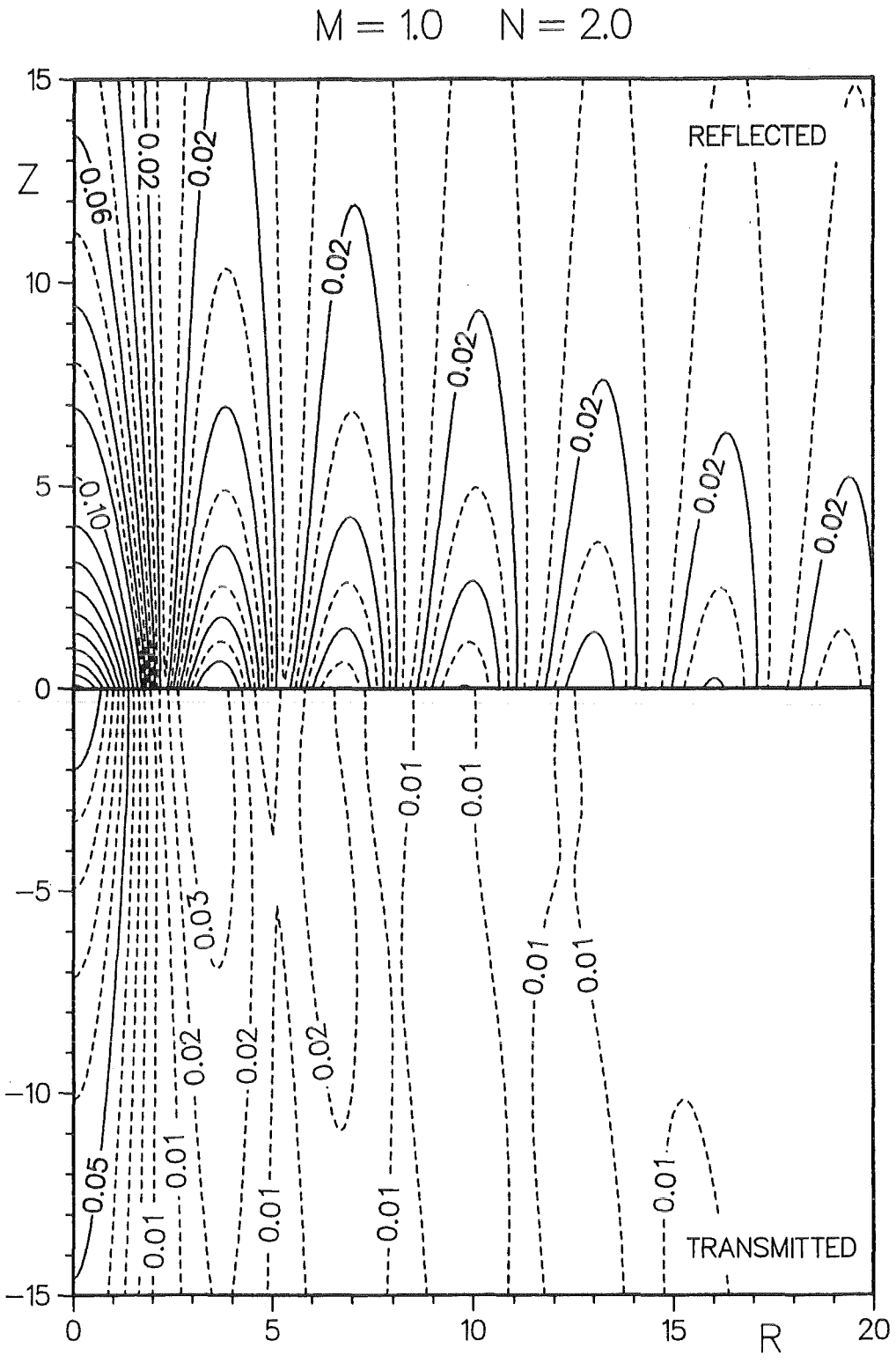

Fig.14: The absolute values of the inhomogeneous components of the Sommerfeld waves for the ratios M and N of densities and phase velocities given above.

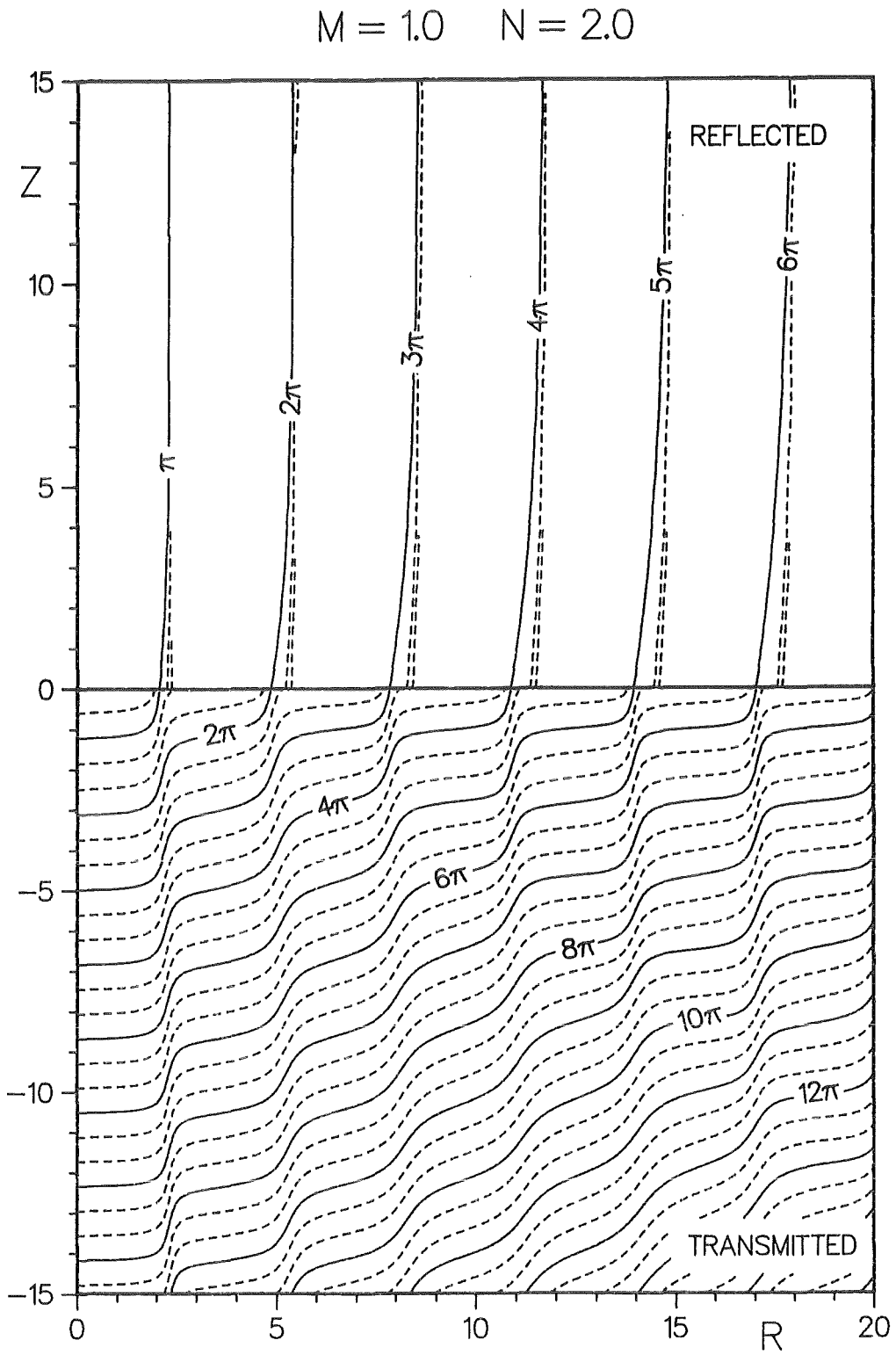

Fig.15: The phase angles of the inhomogeneous components of the Sommerfeld waves for the ratios M and N of densities and phase velocities given above.

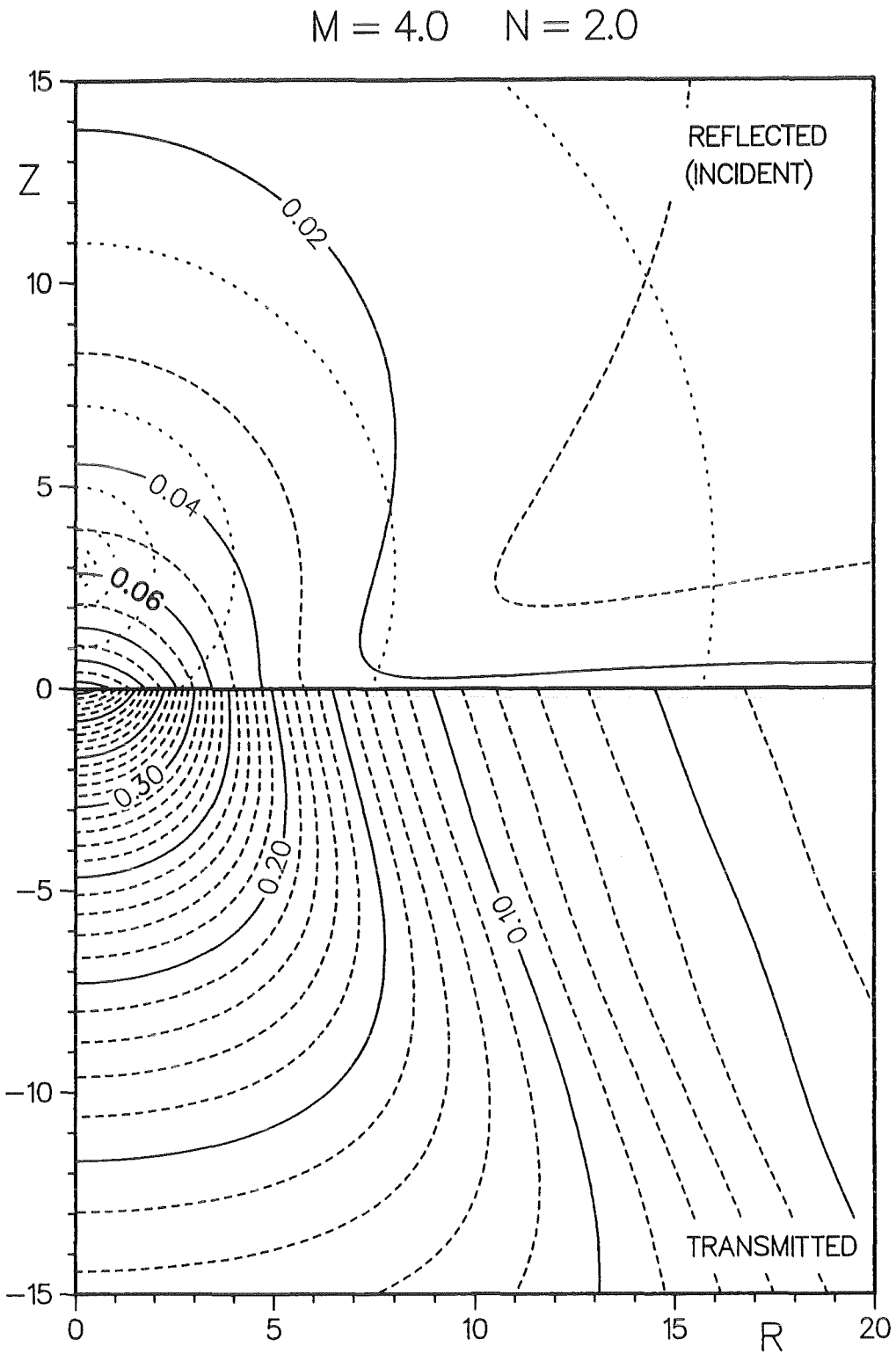

Fig.16: The absolute values of the reflected and transmitted Sommerfeld waves for the ratios M and N of densities and phase velocities given above. For labels of the indicated incident wave, see Fig.6a.

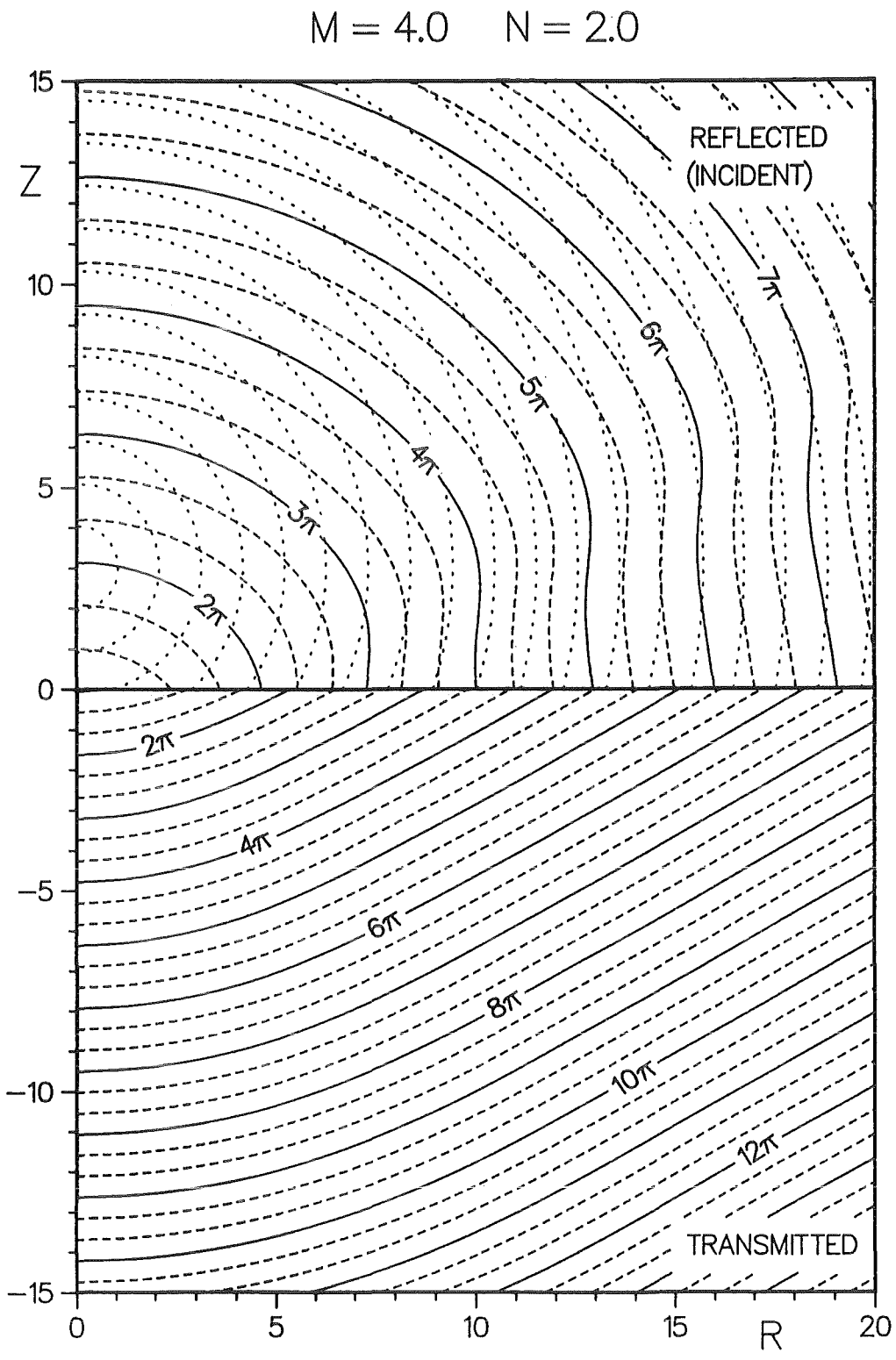

Fig.17: Phase angle of the reflected and transmitted Sommerfeld waves for the ratios M and N of densities and phase velocities given above. For labels of the indicated incident wave, see Fig.6b.

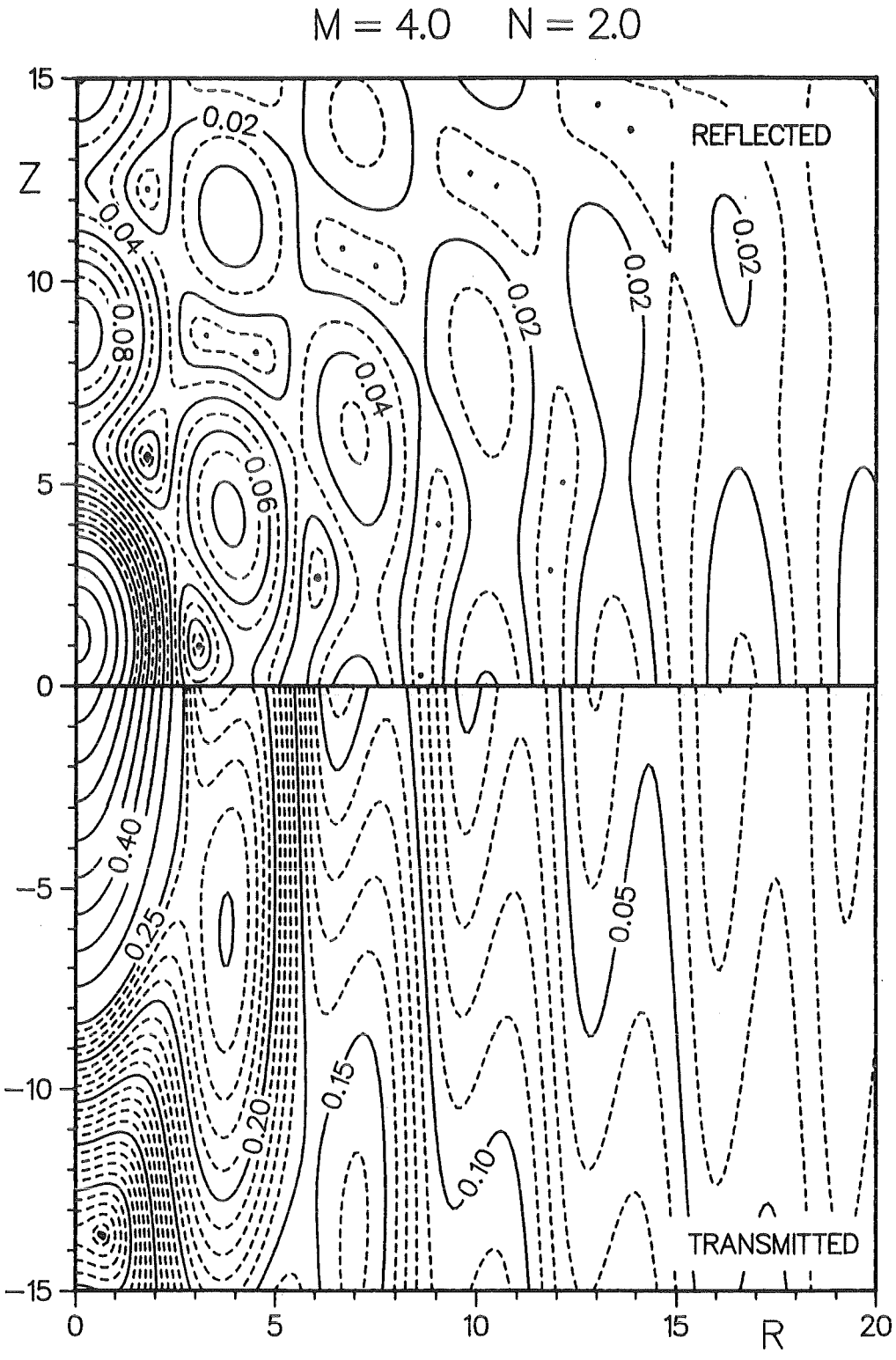

Fig.18: The absolute values of the homogeneous components of the Sommerfeld waves for the ratios M and N of densities and phase velocities given above.

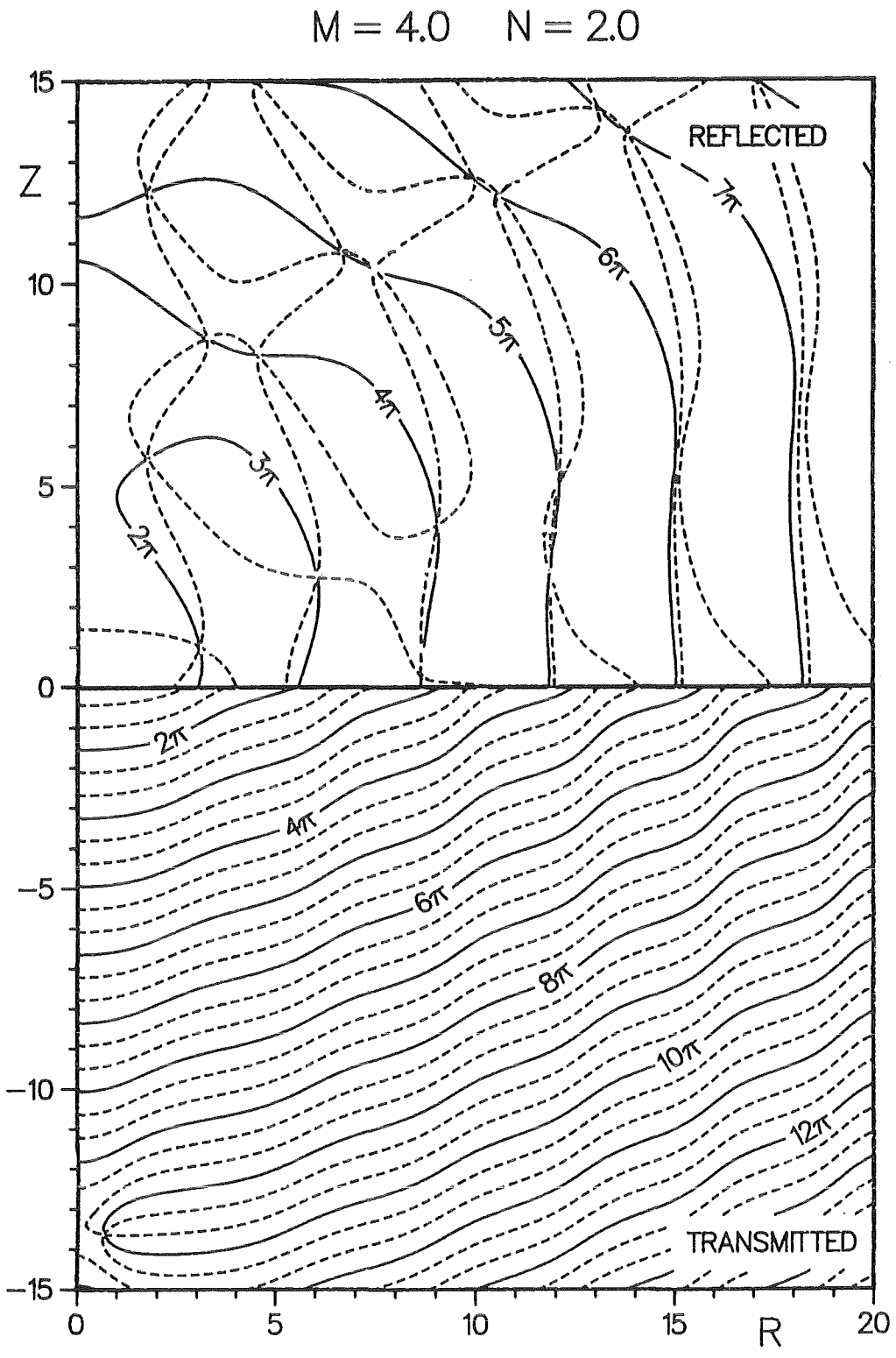

Fig.19: The phase angles of the homogeneous components of the Sommerfeld waves for the ratios M and N of densities and phase velocities given above.

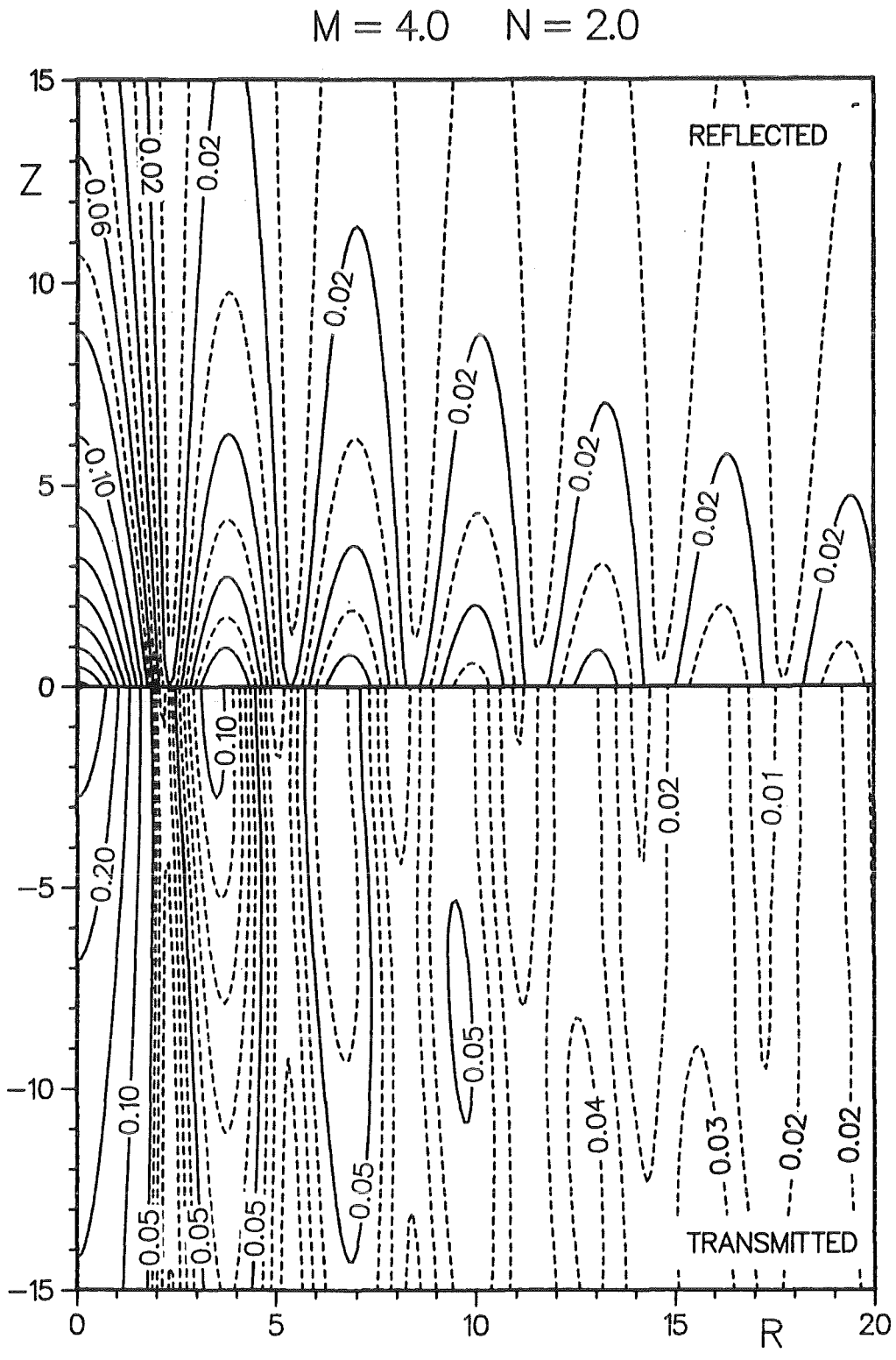

Fig.20: The absolute values of the inhomogeneous components of the Sommerfeld waves for the ratios M and N of densities and phase velocities given above.

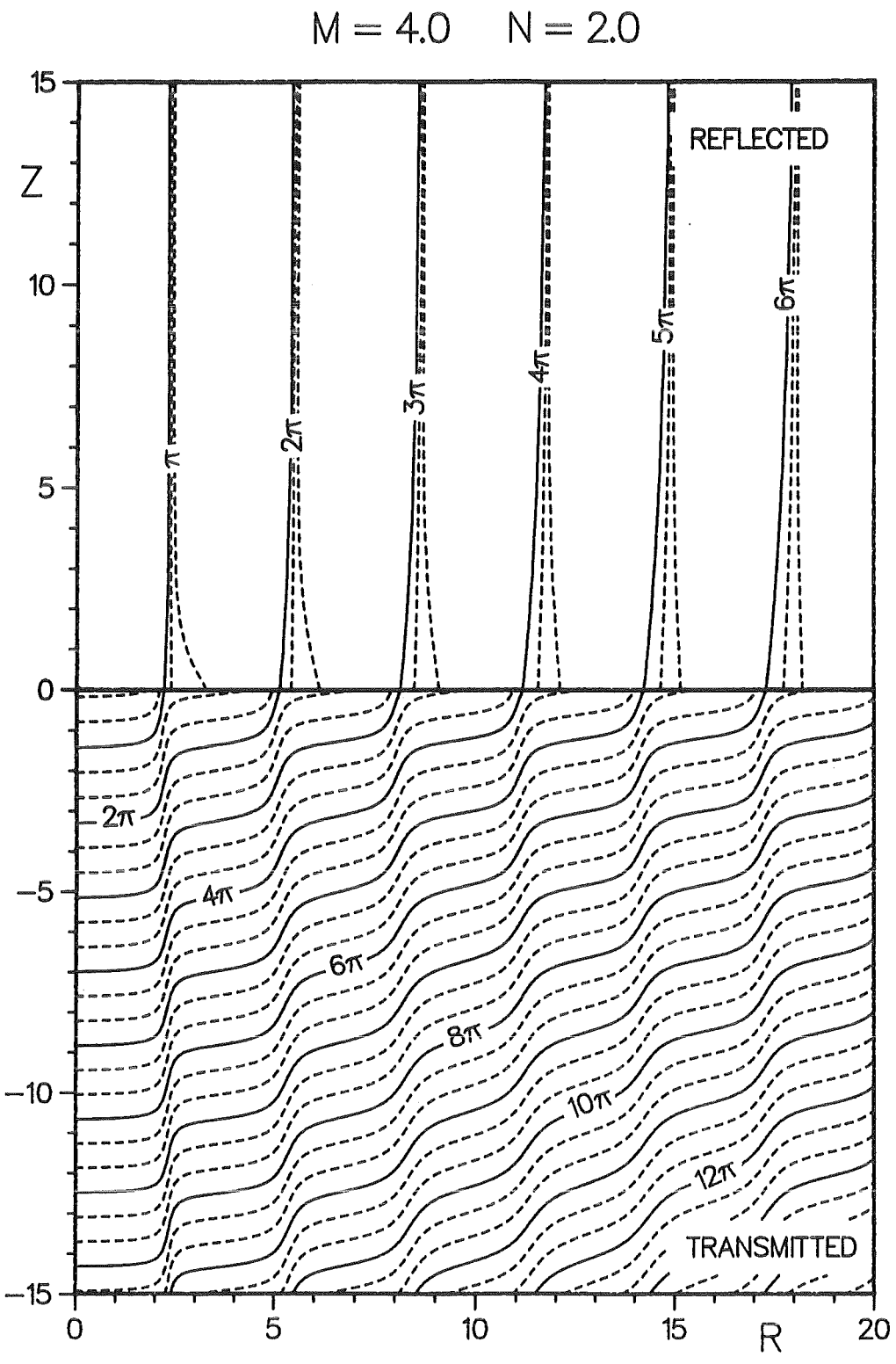

Fig.21: The phase angles of the inhomogeneous components of the Sommerfeld waves for the ratios M and N of densities and phase velocities given above.

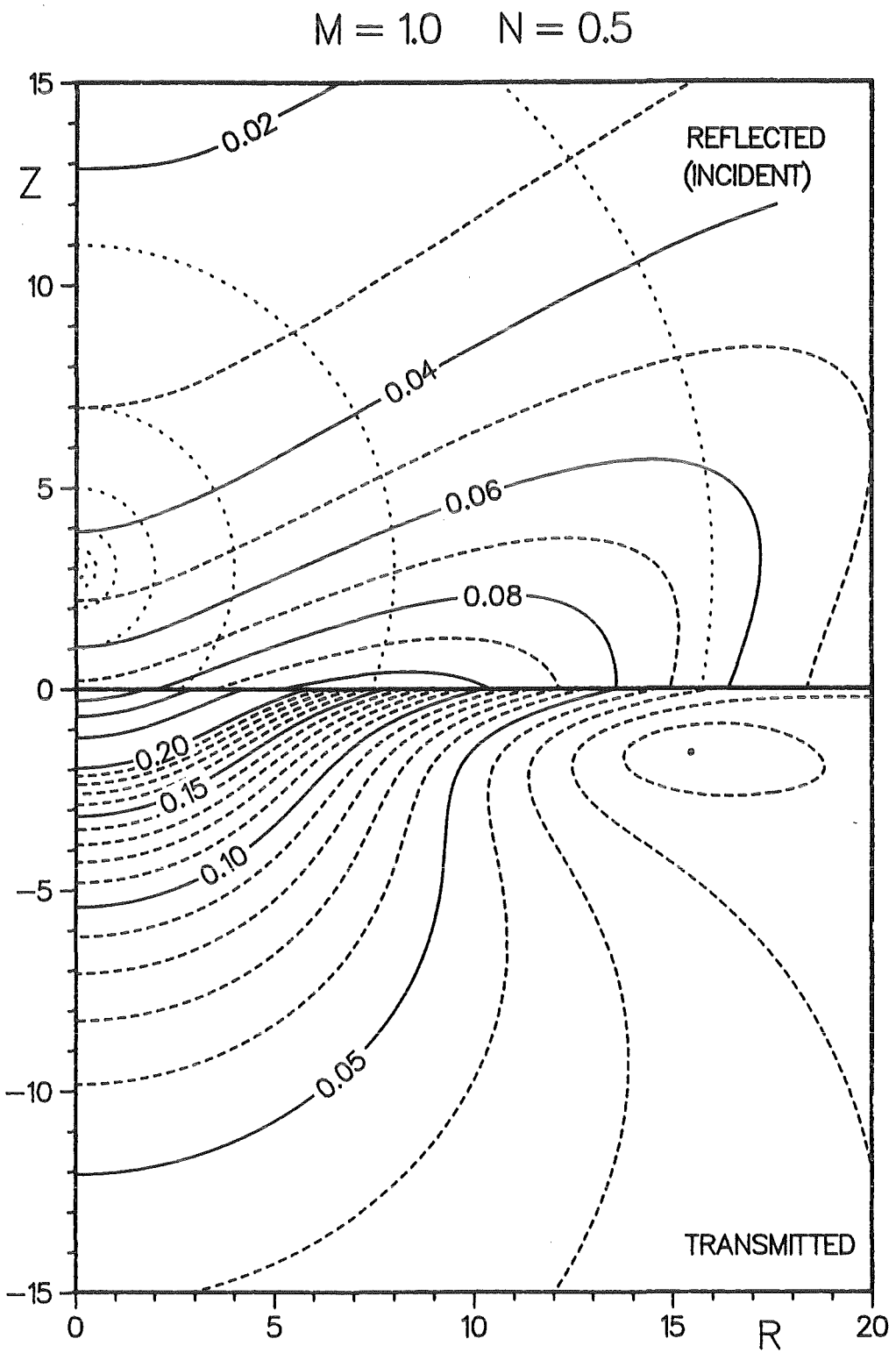

Fig.22: The absolute values of the reflected and transmitted Sommerfeld waves for the ratios M and N of densities and phase velocities given above. For labels of the indicated incident wave, see Fig.6a.

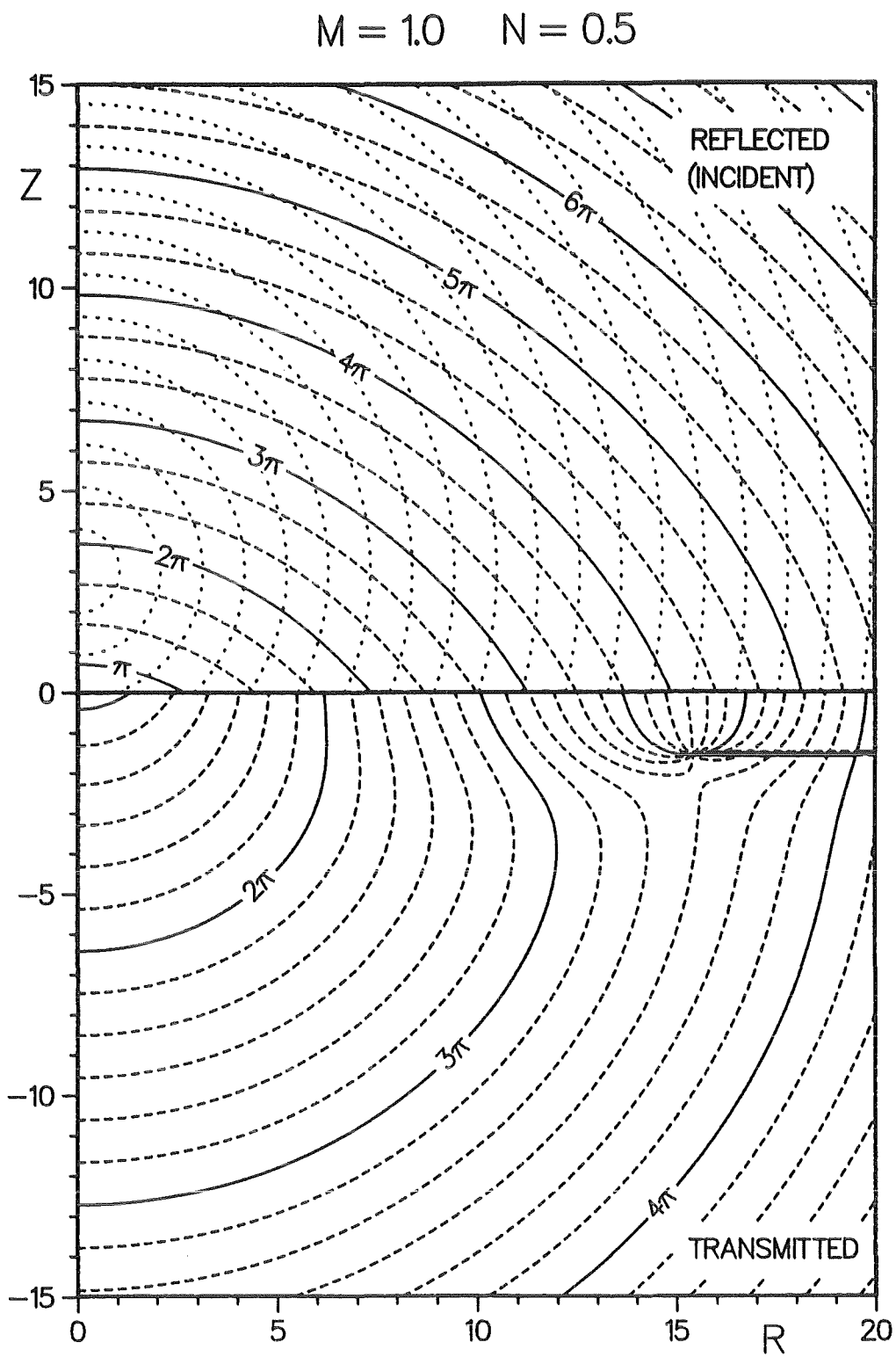

Fig.23: Phase angle of the reflected and transmitted Sommerfeld waves for the ratios M and N of densities and phase velocities given above. For labels of the indicated incident wave, see Fig.6b.

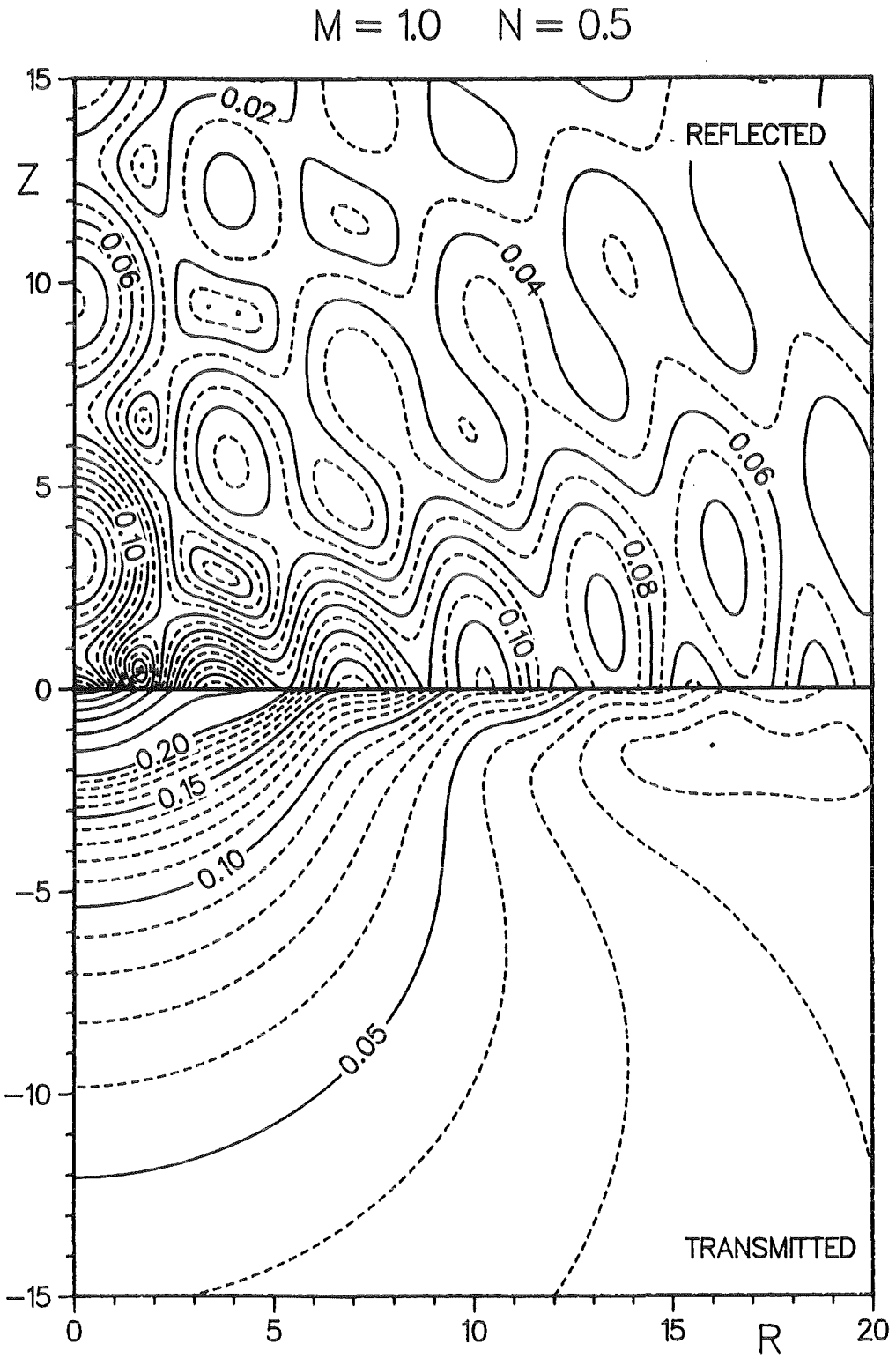

Fig.24: The absolute values of the homogeneous components of the Sommerfeld waves for the ratios M and N of densities and phase velocities given above.

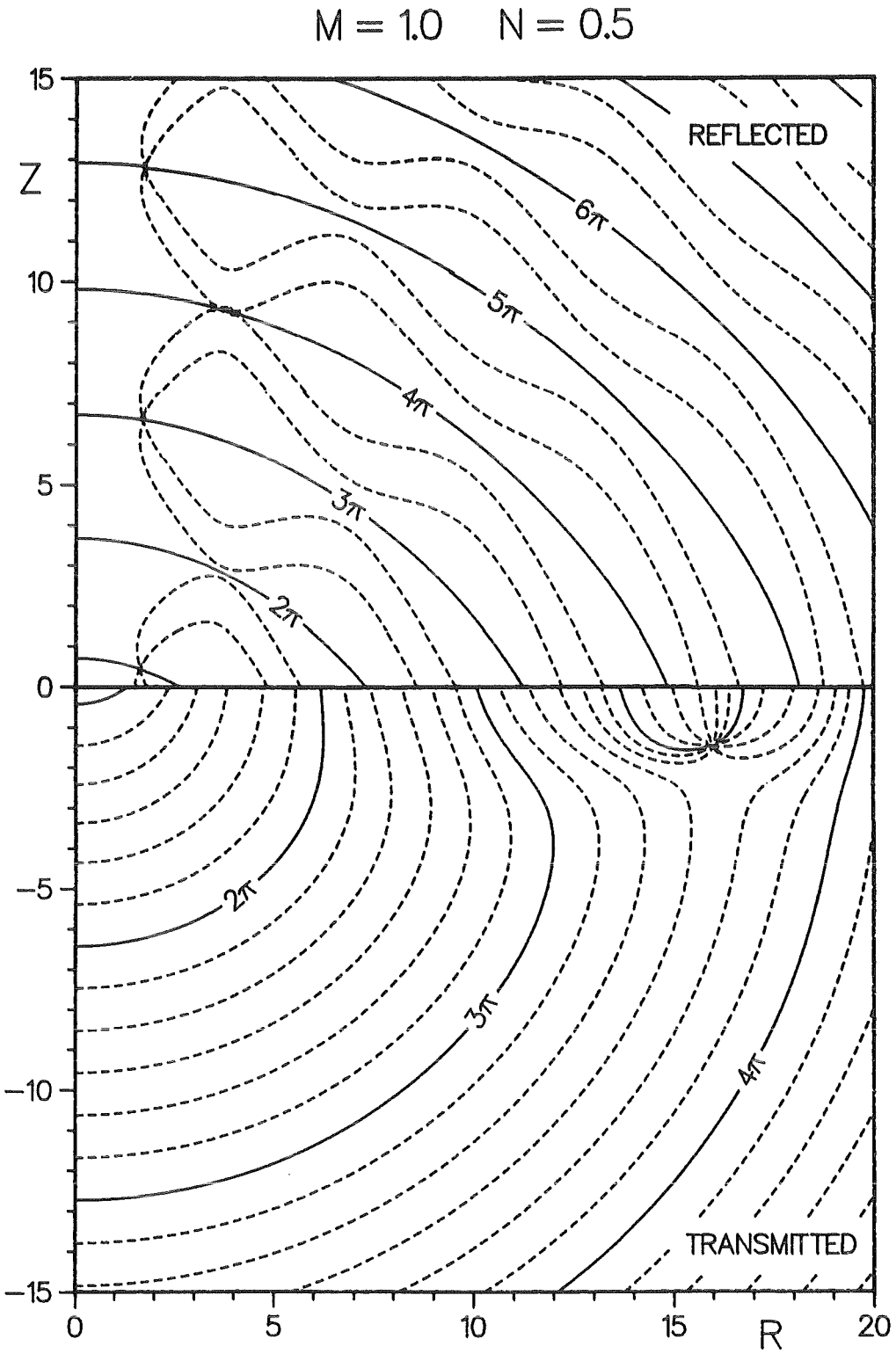

Fig.25: The phase angles of the homogeneous components of the Sommerfeld waves for the ratios M and N of densities and phase velocities given above.

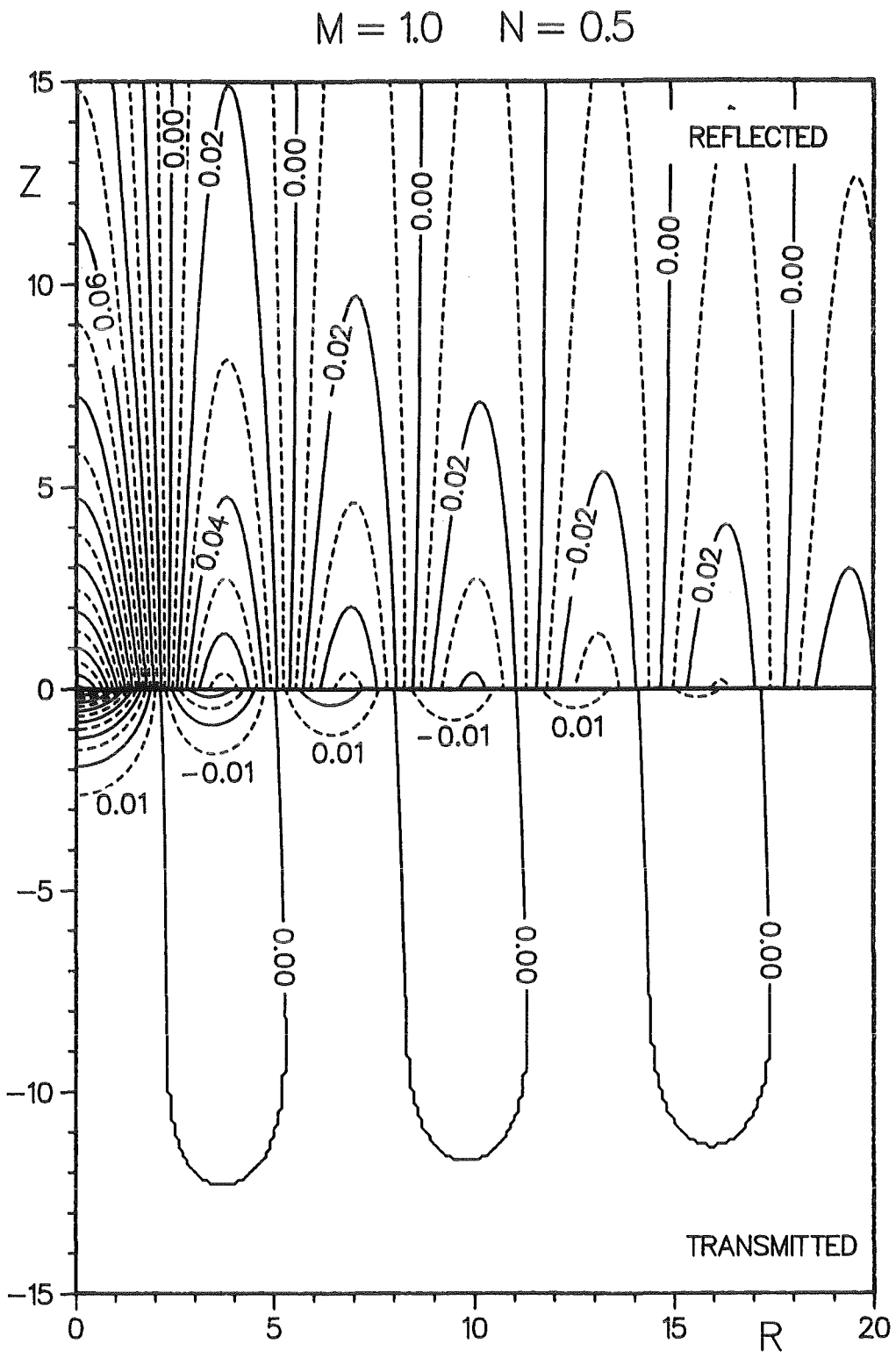

Fig.26: The inhomogeneous components of the Sommerfeld waves for the ratios M and N of densities and phase velocities given above.

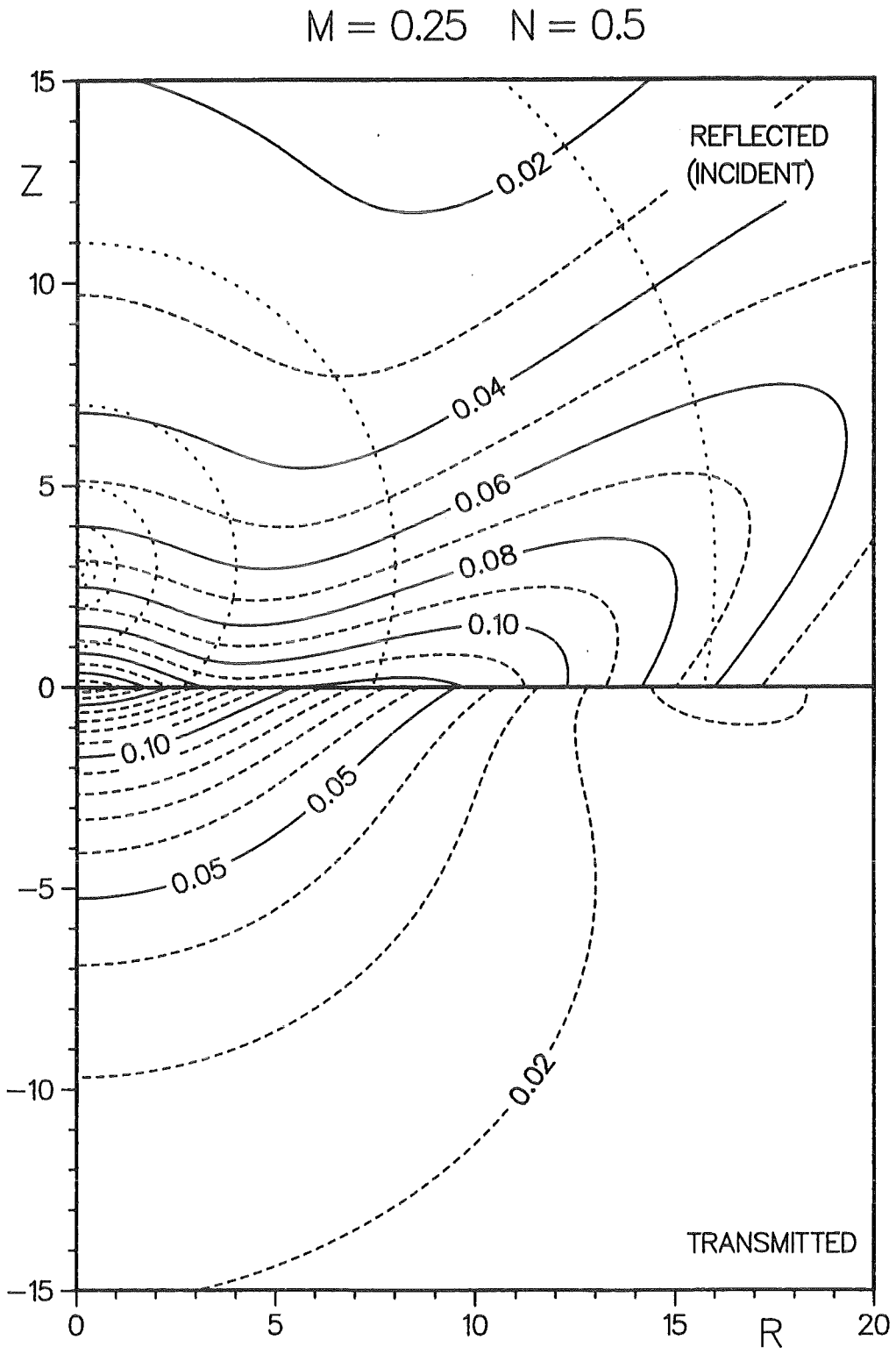

Fig.27: The absolute values of the reflected and transmitted Sommerfeld waves for the ratios M and N of densities and phase velocities given above. For labels of the indicated incident wave, see Fig.6a.

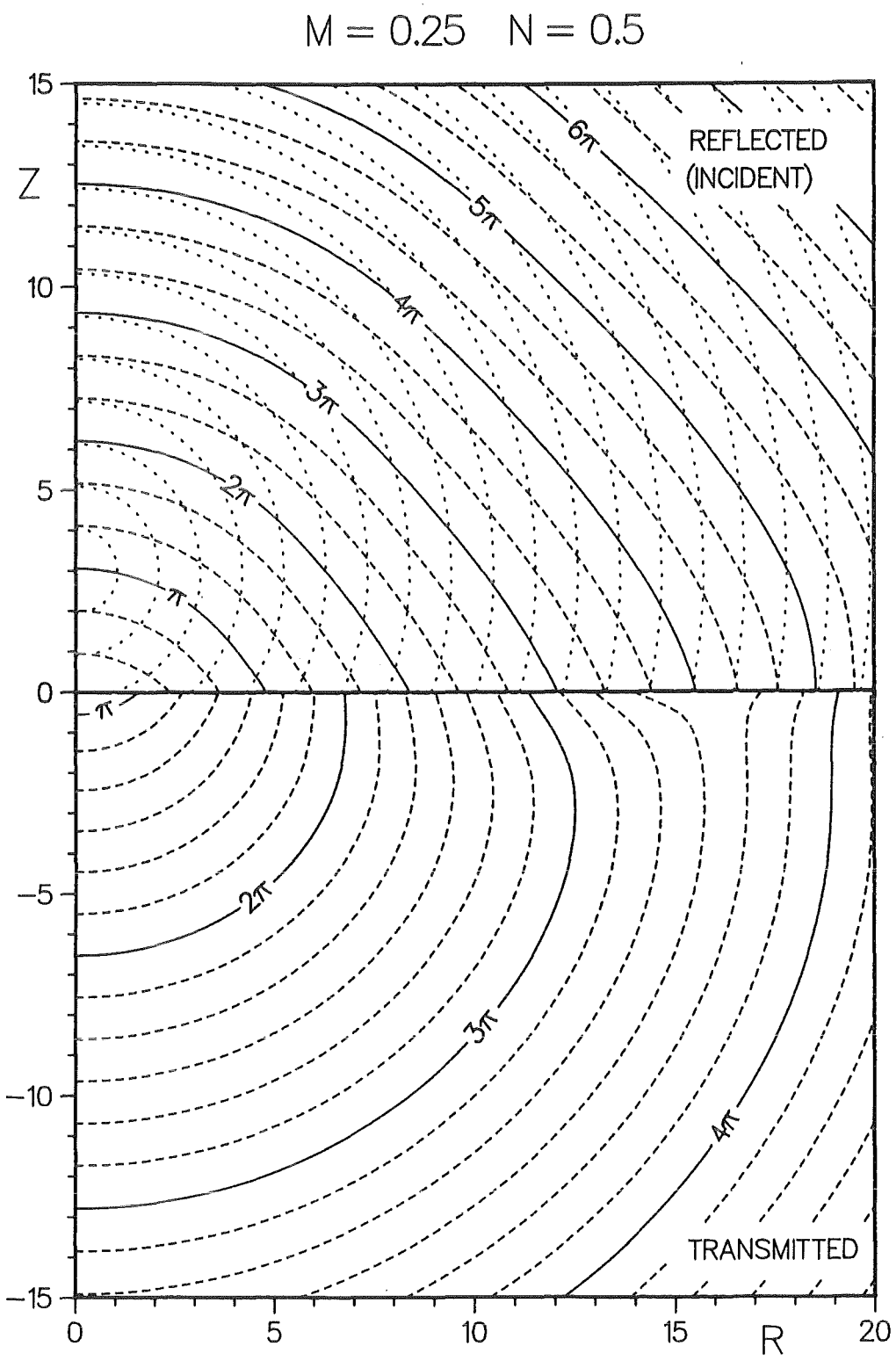

Fig.28: Phase angle of the reflected and transmitted Sommerfeld waves for the ratios M and N of densities and phase velocities given above. For labels of the indicated incident wave, see Fig.6b.

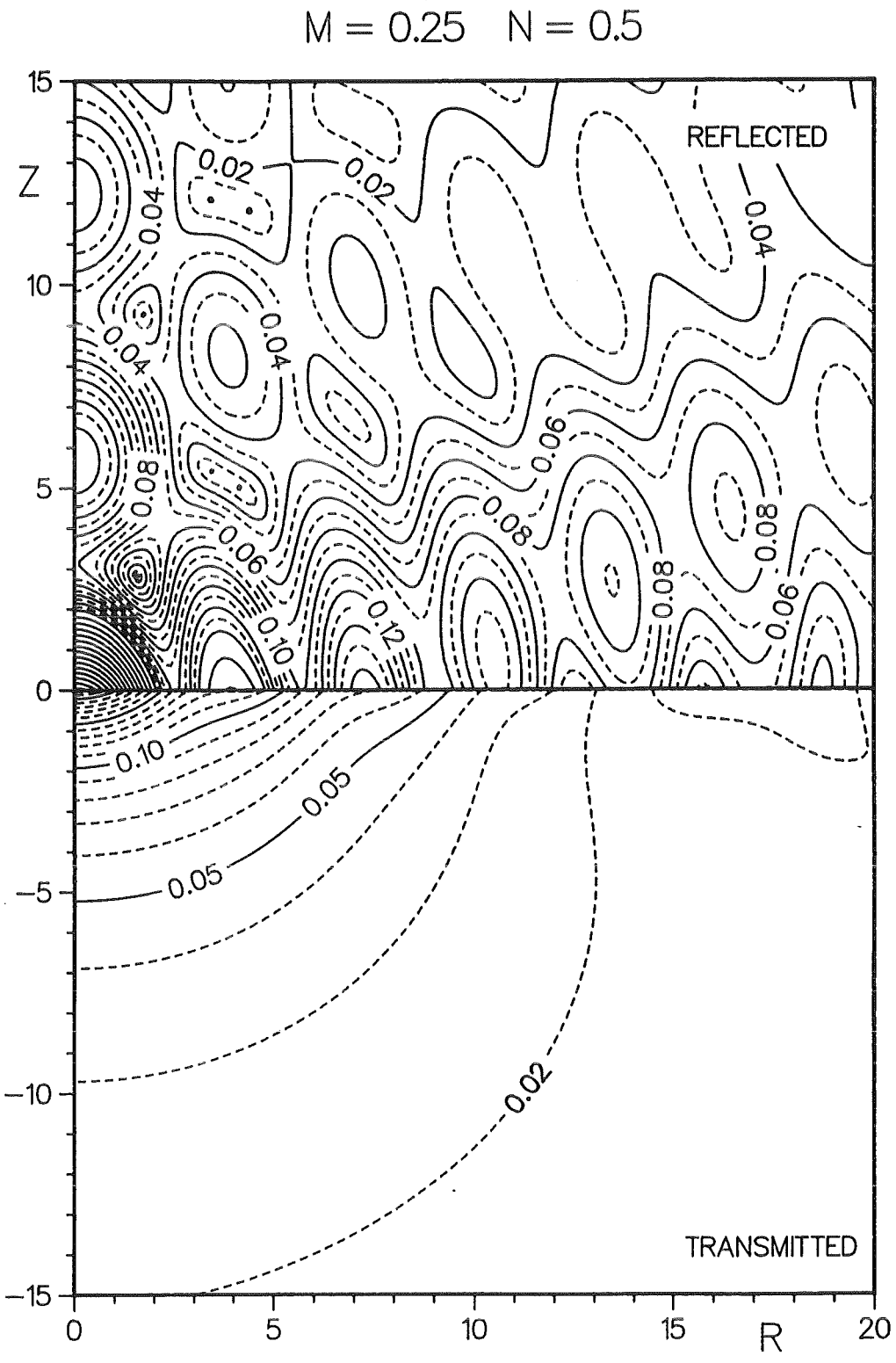

Fig.29: The absolute values of the homogeneous components of the Sommerfeld waves for the ratios M and N of densities and phase velocities given above.

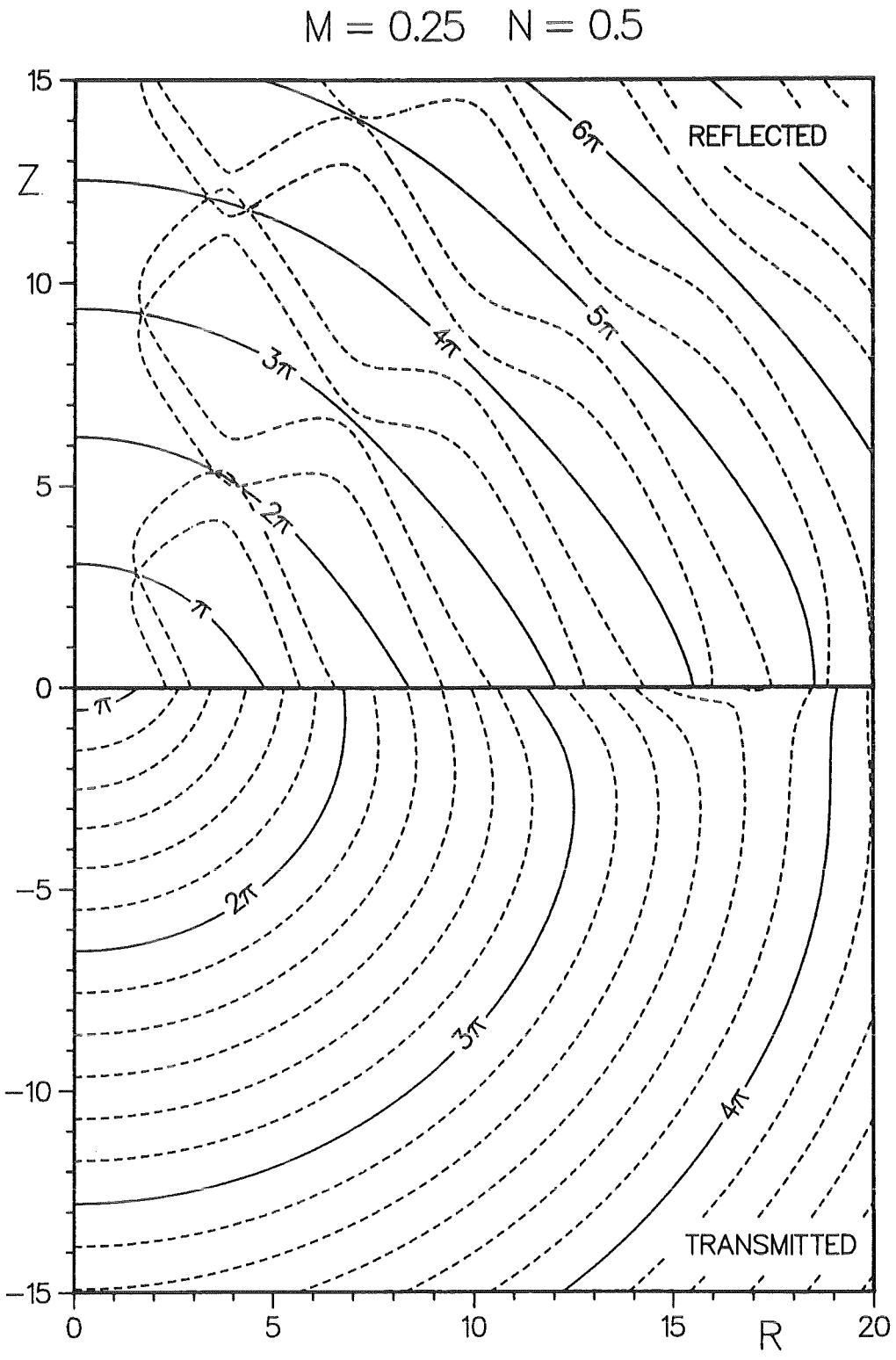

Fig.30: The phase angles of the homogeneous components of the Sommerfeld waves for the ratios M and N of densities and phase velocities given above.

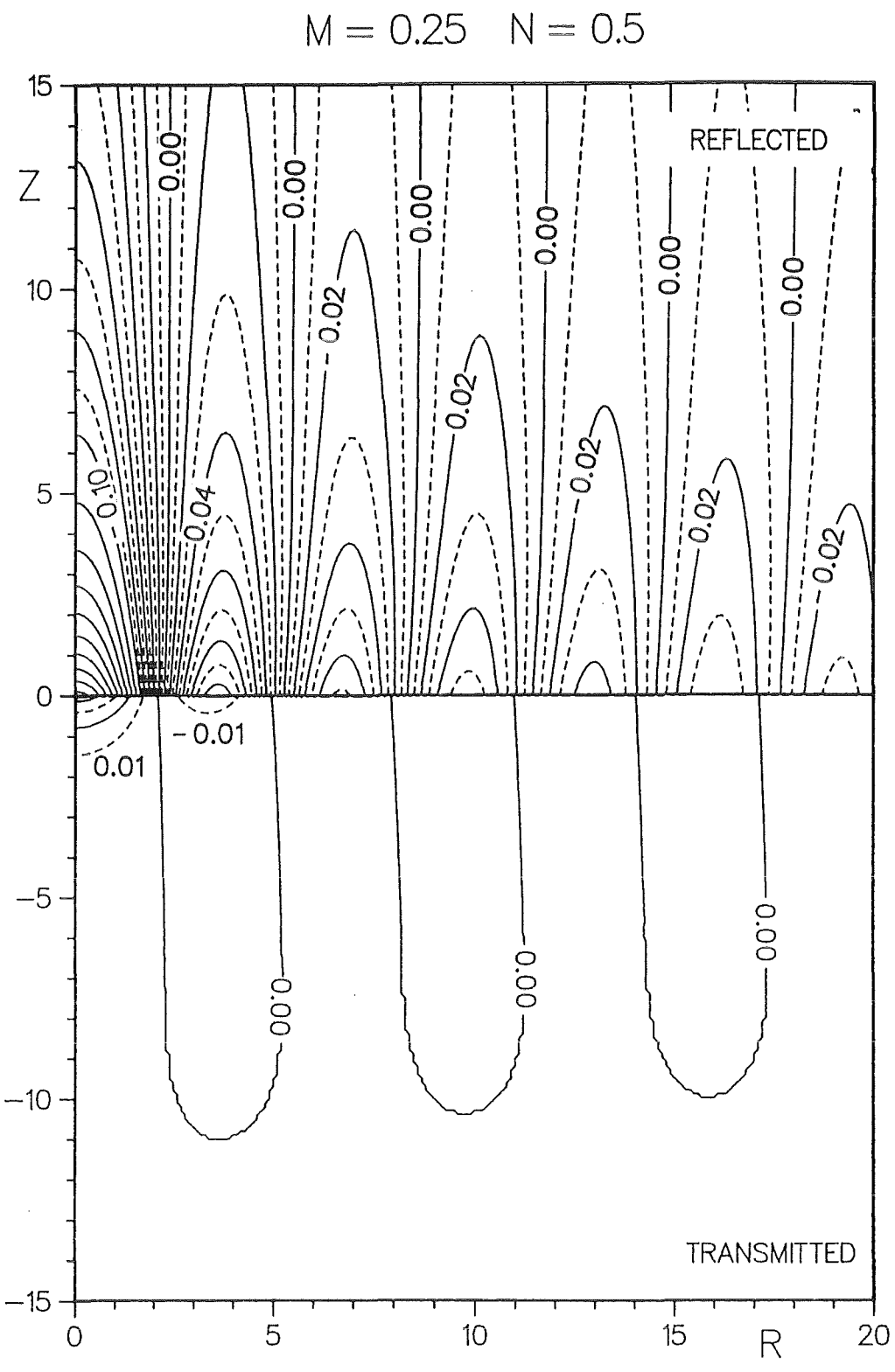

Fig.31: The inhomogeneous components of the Sommerfeld waves for the ratios M and N of densities and phase velocities given above.

6.3 *RTA waves for reflection and transmission*

These waves are calculated following Eqs. (5.3) and (5.6). Results are shown in Figs. 32 to 37. By the use of Fresnel coefficients (2.16), (2.17) the kinematic and dynamic boundary conditions (2.11) and (2.14) are automatically fulfilled. However, the Helmholtz equation (2.2) must be expected to be violated. To demonstrate this effect, the relative violation of Eq. (2.2)

$$|\Delta PR + PR|/|PR| \ , \tag{6.1}$$

$$|\Delta PT + N^2 PT|/|PT| \tag{6.2}$$

for reflected and transmitted RTA waves are plotted in Figs. 34 and 37.

The case $M=1, N=2$ (Figs. 32 to 34) corresponds to Fig. 3b for plane waves. In Fig. 33 the negative sign of the local reflection coefficient V, Eq. (2.16), is described by a shift by $-\pi$ of PR with respect to the incident wave PI. The relative violation of the Helmholtz equation is shown in Fig. 34. It reaches as much as about 25 per cent for PR and PT at the origin $R=Z=0$.

The case $M=4, N=2$ (Figs. 35 to 37) corresponds to Fig. 3a for plane waves. At the line

$$R = 2(Z + Z0) \tag{6.3}$$

for $Z0=3$, $Z \geq 0$ the local reflection coefficient V, Eq. (2.16) vanishes and the phase angle of PR has a discontinuity of π as is shown in Fig. 35 and 36. The relative violation of the Helmholtz equation is shown in Fig. 37. For PR the maximum is about 35 per cent at $R=5$, $Z=0$, for PT it is about 20 per cent at the origin.

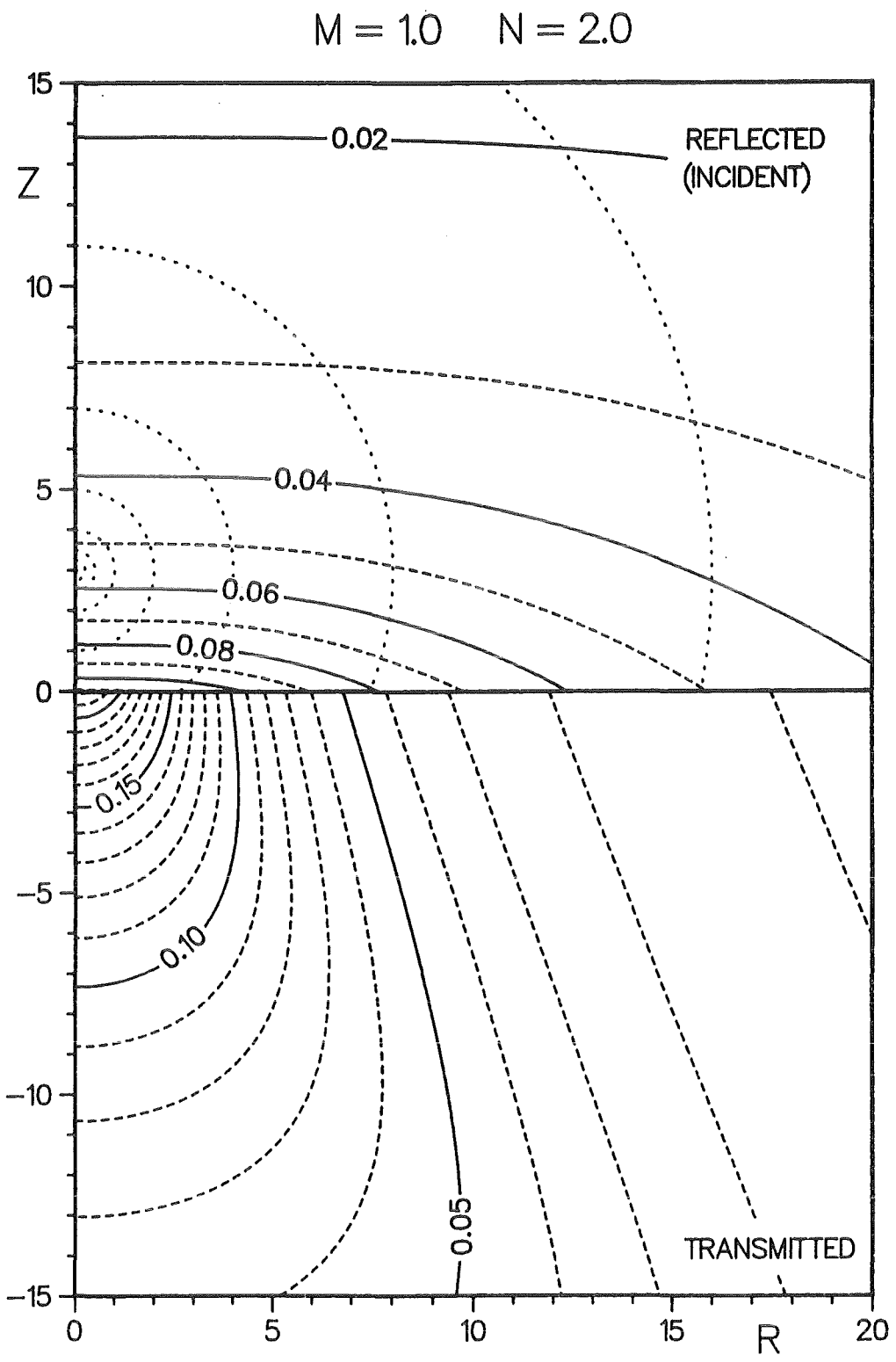

Fig.32: The absolute values of the reflected and transmitted RTA waves for the ratios M and N of densities and phase velocities given above. For labels of the indicated incident wave, see Fig.6a.

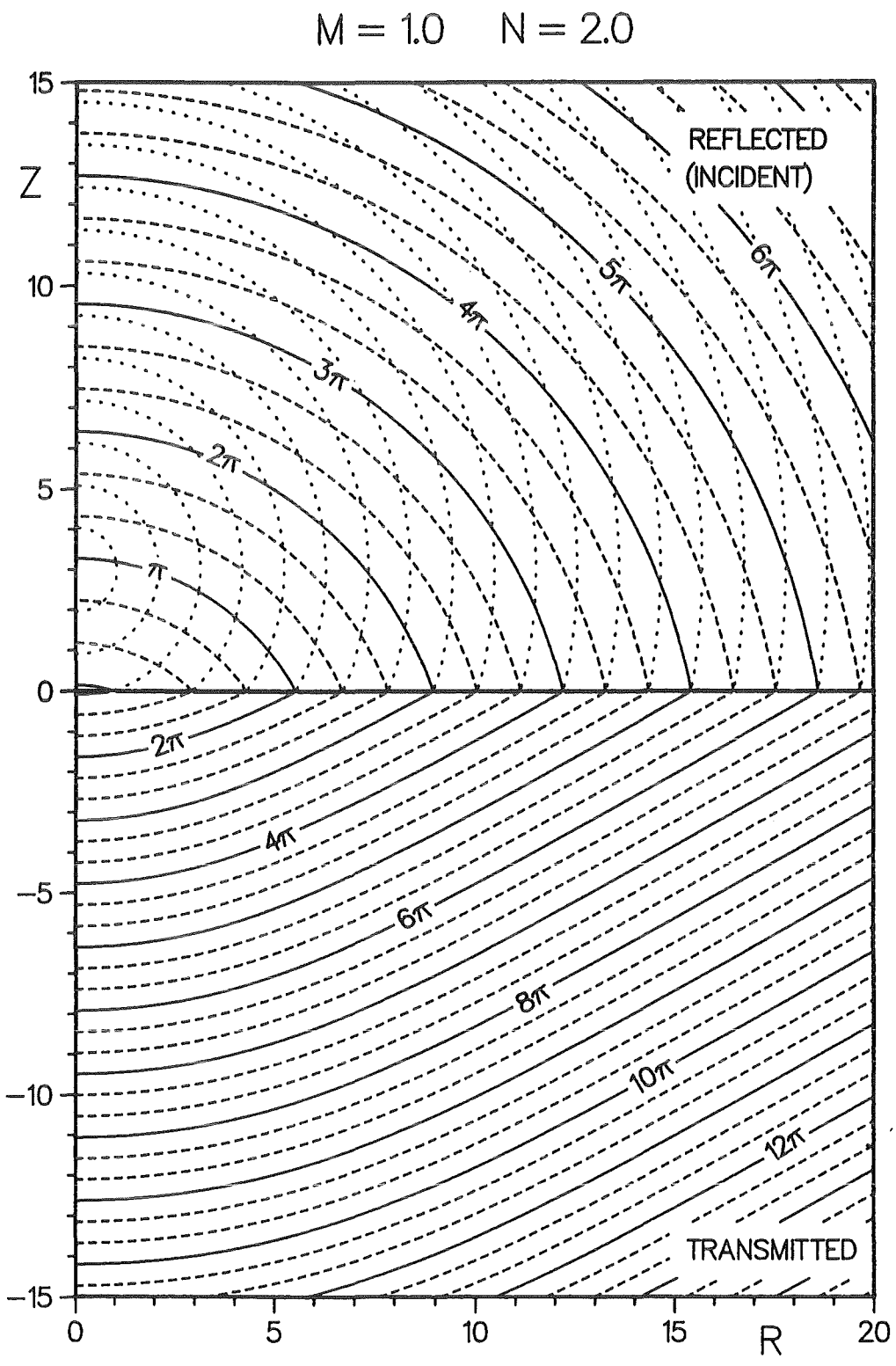

Fig.33: The phase angles of the reflected and transmitted RTA waves for the ratios M and N of densities and phase velocities given above. For labels of the indicated incident wave, see Fig.6b.

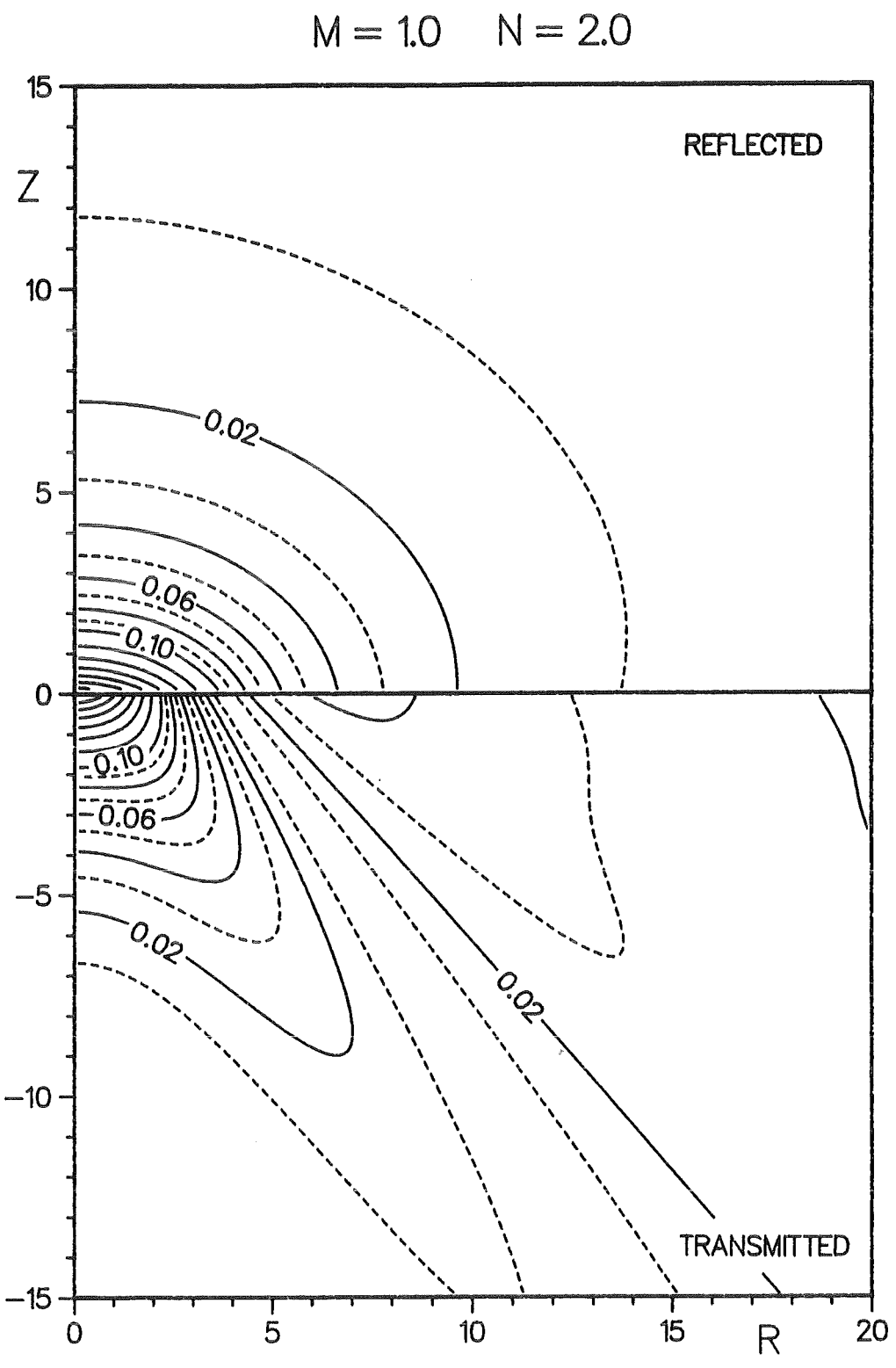

Fig.34: Relative violation of the Helmholtz equation by RTA waves for the ratios M and N of densities and phase velocities given above. For definition, see expressions (6.1) and (6.2).

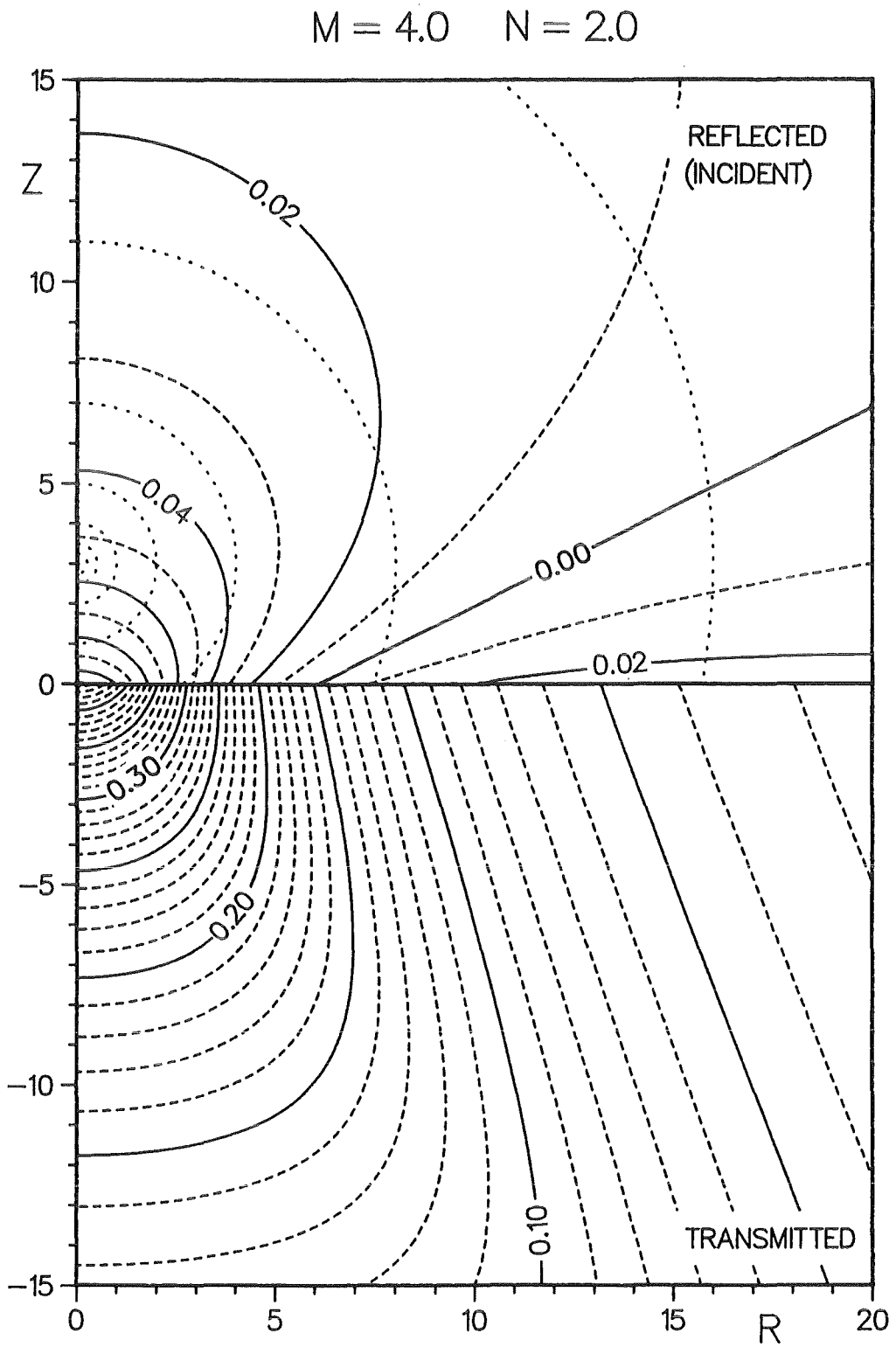

Fig.35: The absolute values of the reflected and transmitted RTA waves for the ratios M and N of densities and phase velocities given above. For labels of the indicated incident wave, see Fig.6a.

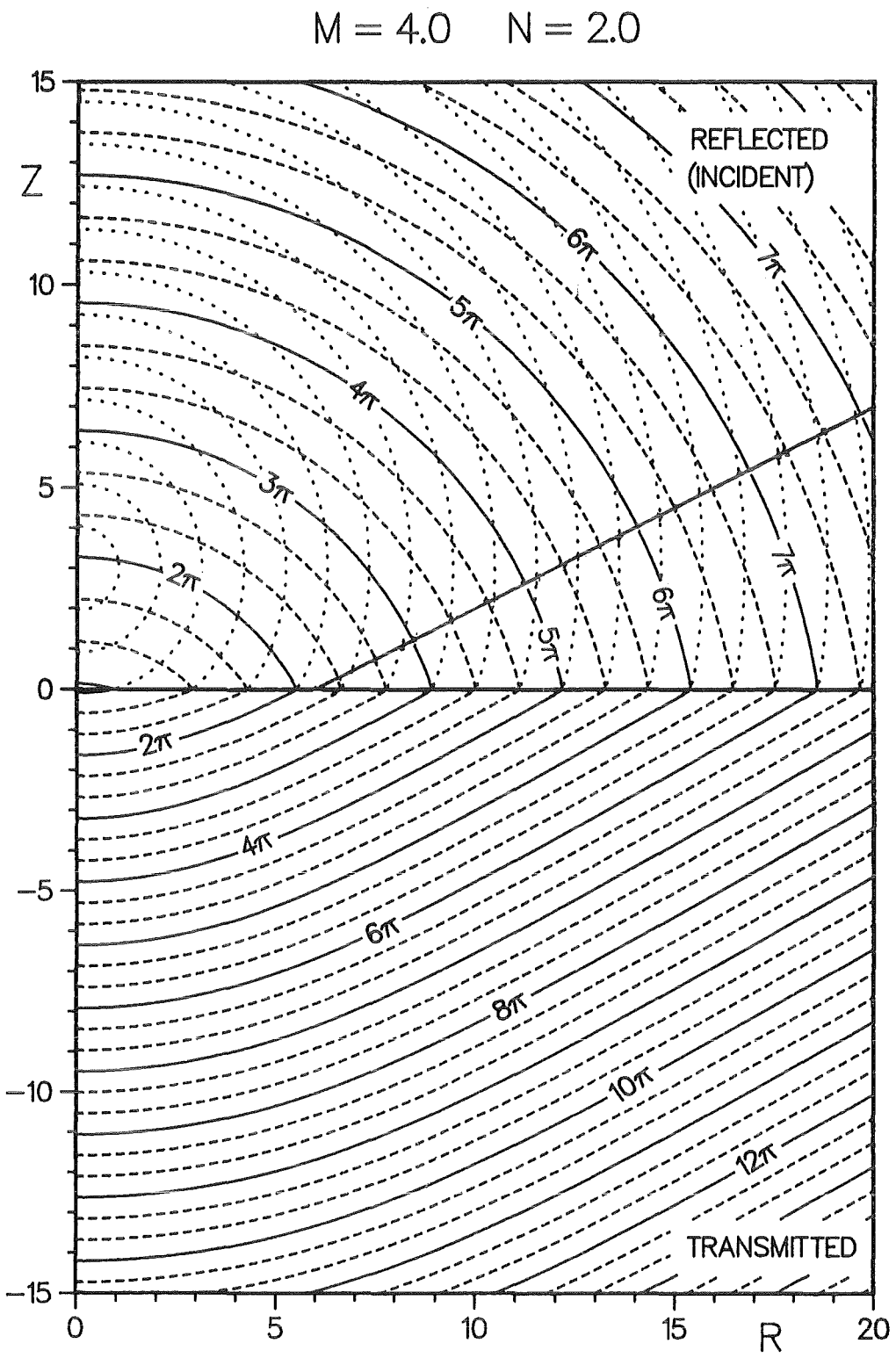

Fig.36: The phase angles of the reflected and transmitted RTA waves for the ratios M and N of densities and phase velocities given above. For labels of the indicated incident wave, see Fig.6b.

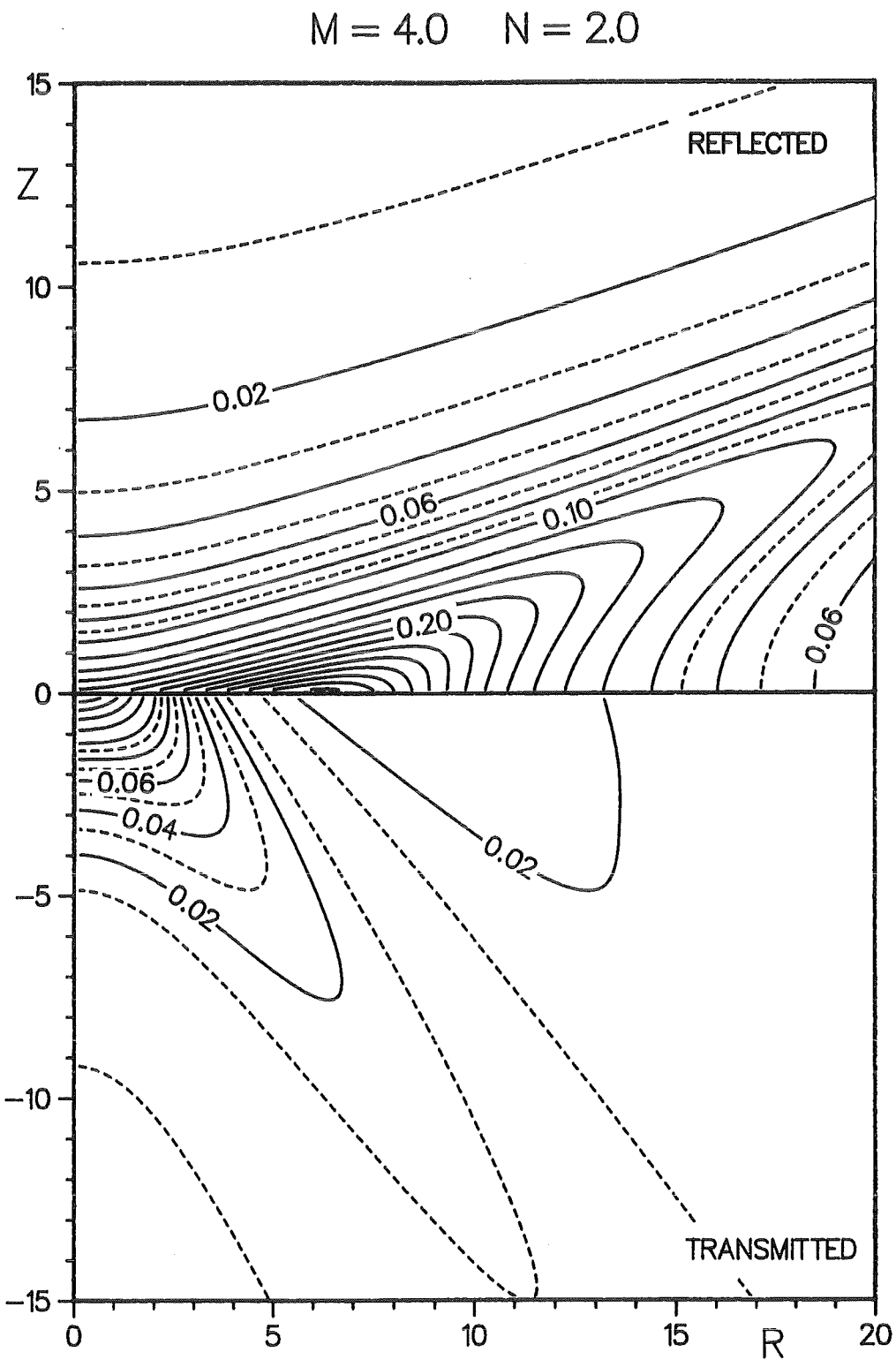

Fig.37: Relative violation of the Helmholtz equation by RTA waves for the ratios M and N of densities and phase velocities given above. For definition, see expressions (6.1) and (6.2).

6.4 *A comparison of RTA with Sommerfeld waves*

The comparisons of these waves are shown in Figs. 38 to 43. As quantities of comparison we use (Y stands for R (reflected) or T (transmitted)):

- the ***relative difference of magnitude***

$$DMYR = (|PY_{RTA}| - |PY_{SOM}|) / |PY_{SOM}| \quad , \tag{6.4}$$

which is shown in Figs. 38 and 42;

- the ***difference of phase angles***

$$D\Phi Y = \Phi_{RTA} - \Phi_{SOM} \quad , \tag{6.5}$$

which is shown in Figs. 39 and 43;

- the ***local reflection coefficient***

$$V_l = PR(R, Z = 0) / PI(R, Z = 0) \quad . \tag{6.6}$$

The magnitude and argument of this coefficient is shown in Figs. 40 and 43.

Since RTA and Sommerfeld waves fulfill the kinematic and dynamic boundary conditions, the local transmission coefficient W_l equals $1 + V_l$.

For the case $M=1, N=2$ RTA are shown in Figs. 32, 33 and Sommerfeld waves in Figs. 10, 11. The relative difference of PR in Fig. 38 seems to vanish along the line $R = 5 (Z+3)/3$ within the computational accuracy. The difference of phase angle $D\Phi R$ (Fig. 39) decreases monotonously with increasing distance from the origin. The local reflection coefficients (Fig. 40) are very similar in magnitude. At $R = 0$ their arguments differ by about 0.3 radian. For this case, ΦR_{RTA} has been increased by 2π with respect to fig. 33.

For the case $M=4, N=2$ RTA waves are shown in Figs. 35, 36 and Sommerfeld waves in Figs. 16, 17. Absolute value and argument of the reflected RTA wave have

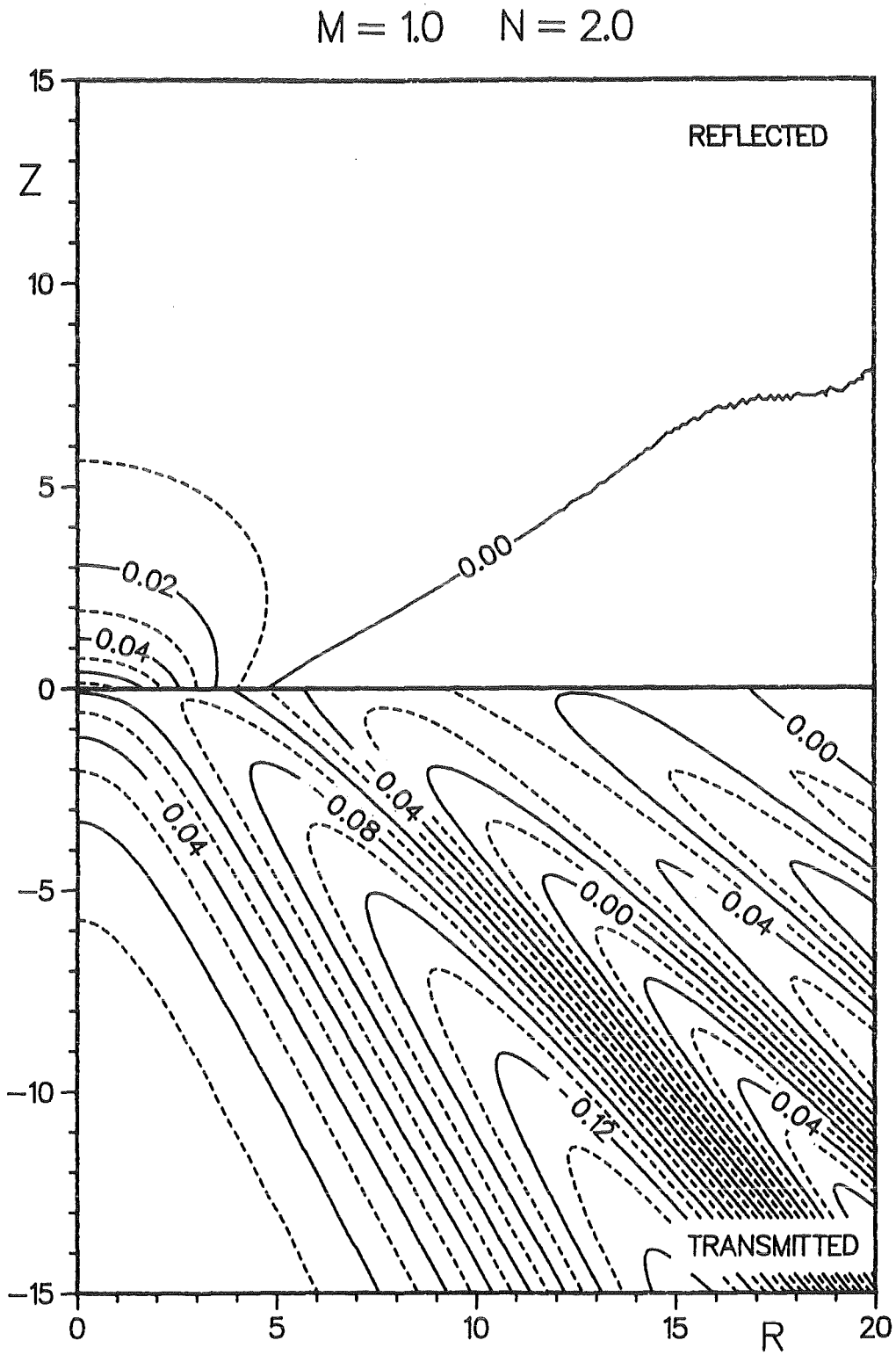

Fig.38: Relative difference of magnitude between RTA and Sommerfeld waves for the ratios M and N of densities and phase velocities given above. For definition, see Eq. (6.4).

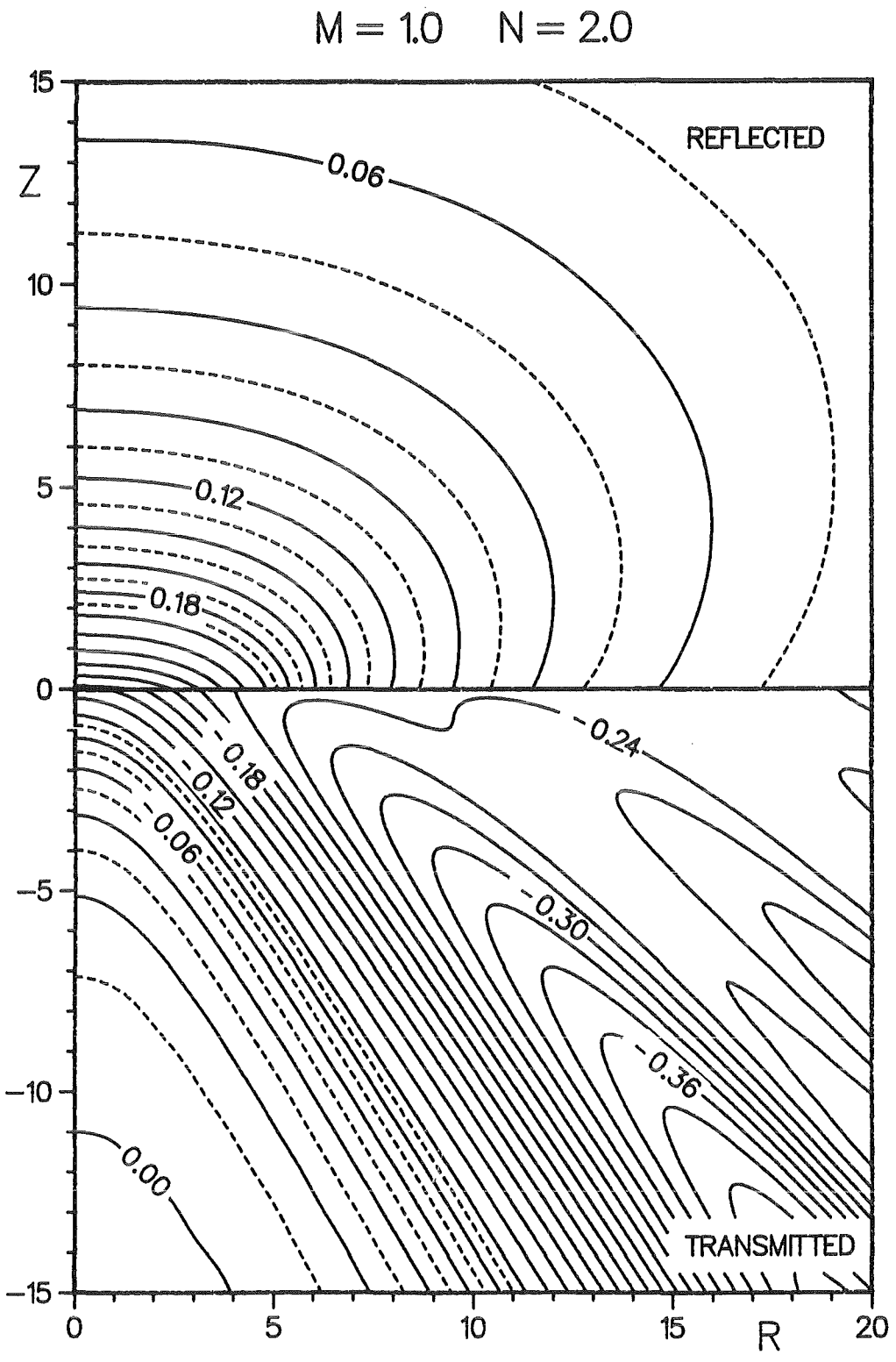

Fig.39: Difference of phase angles (in radian) between RTA and Sommerfeld waves for the ratios M and N of densities and phase velocities given above. For definition, see Eq. (6.5).

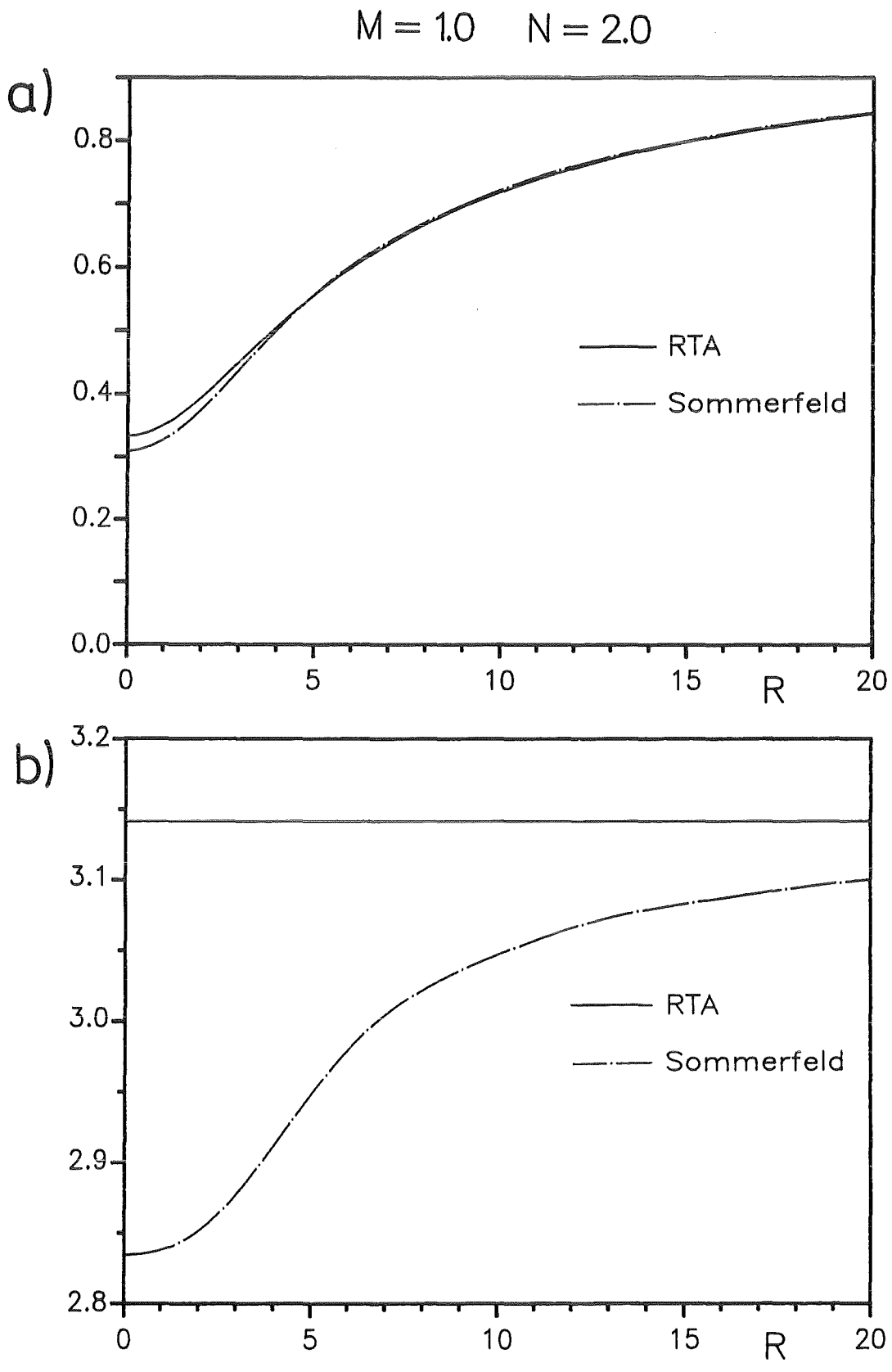

Fig.40: Magnitude (a) and argument (b) (in radian) of the local reflection coefficient for RTA and Sommerfeld waves for the ratios M and N of densities and phase velocities given above. For definition, see Eq. (6.6).

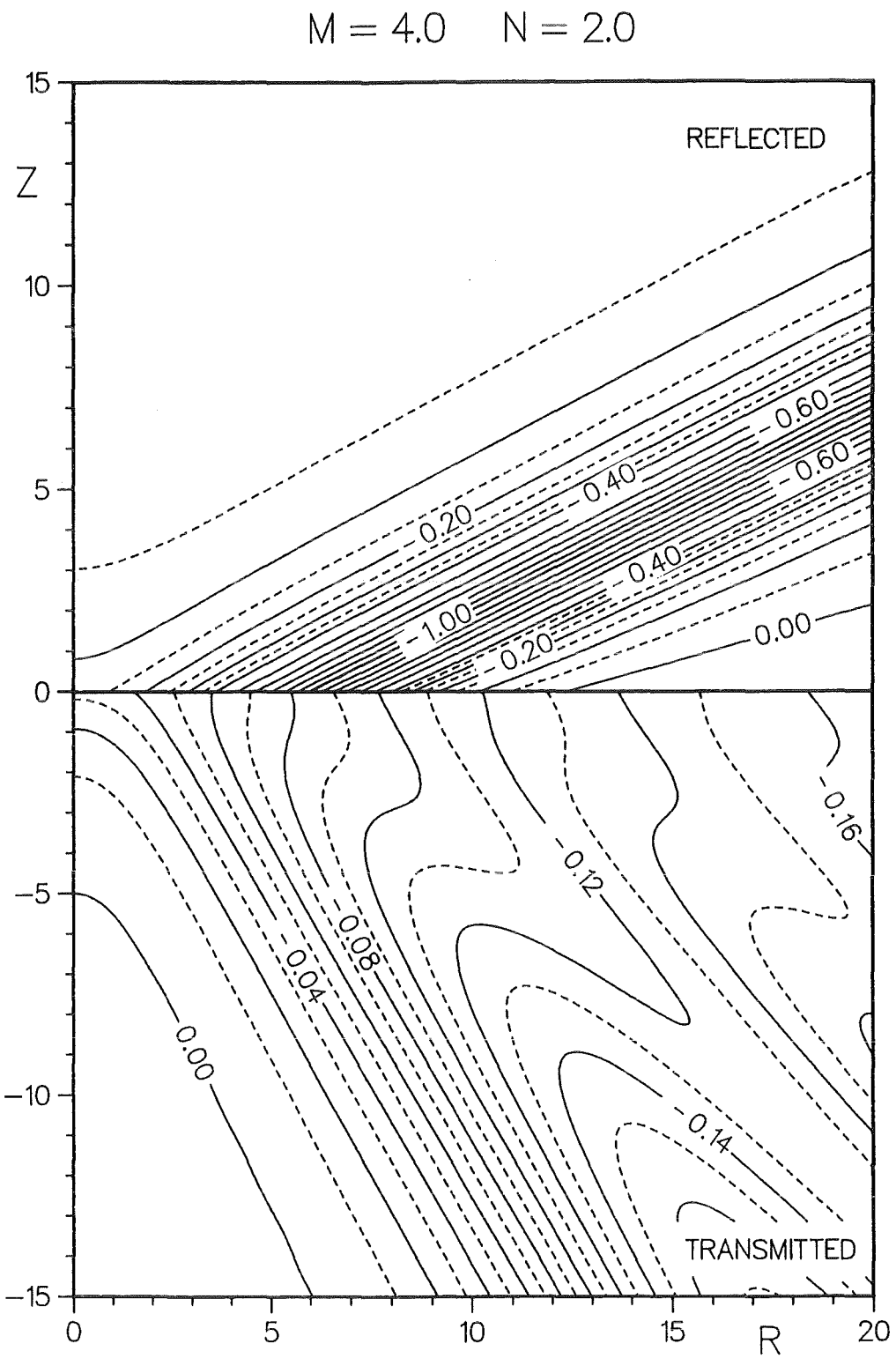

Fig.41: Relative difference of magnitude between RTA and Sommerfeld waves for the ratios M and N of densities and phase velocities given above. For definition, see Eq. (6.4).

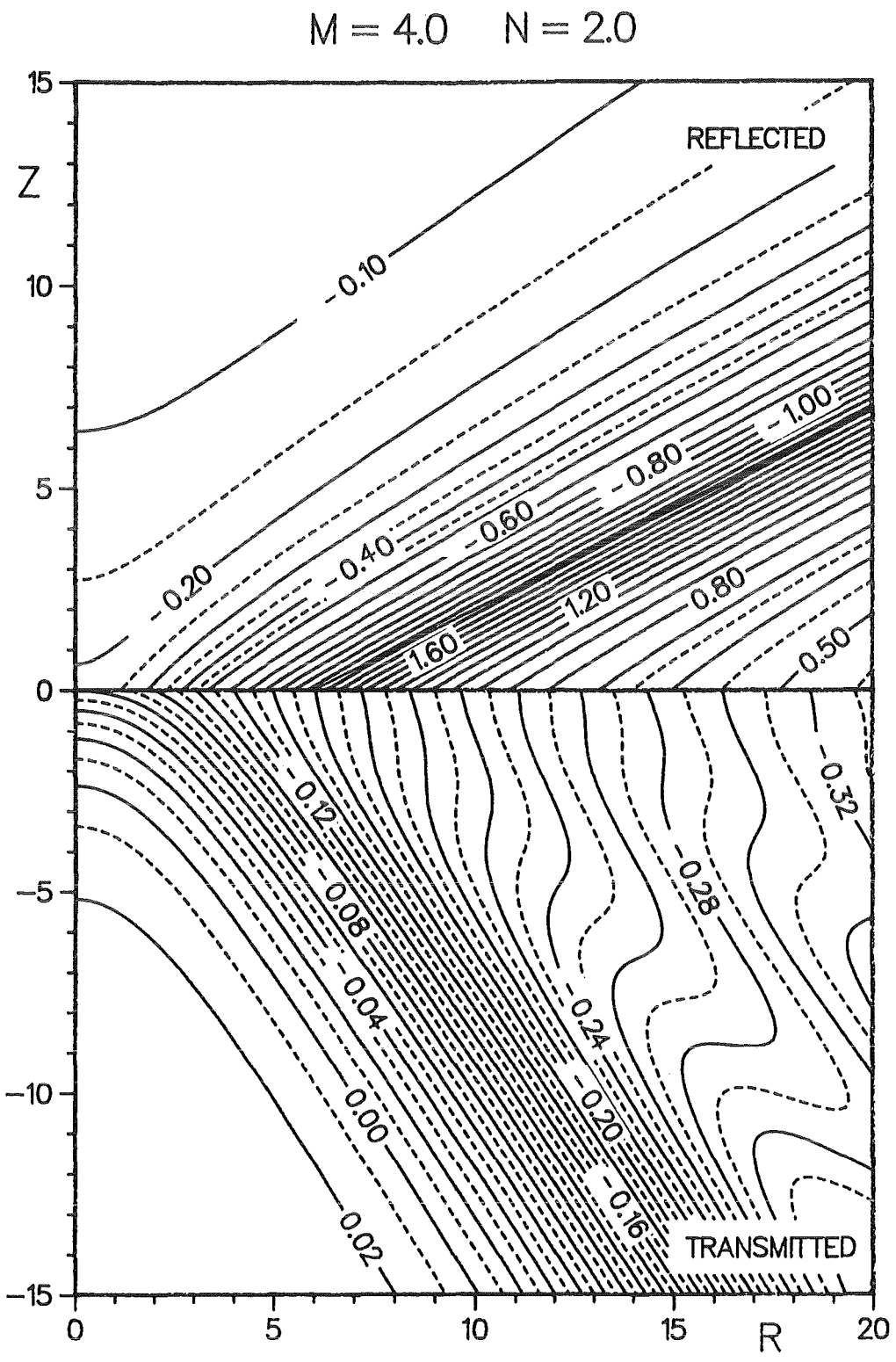

Fig.42: Difference of phase angles (in radian) between RTA and Sommerfeld waves for the ratios M and N of densities and phase velocities given above. For definition, see Eq. (6.5).

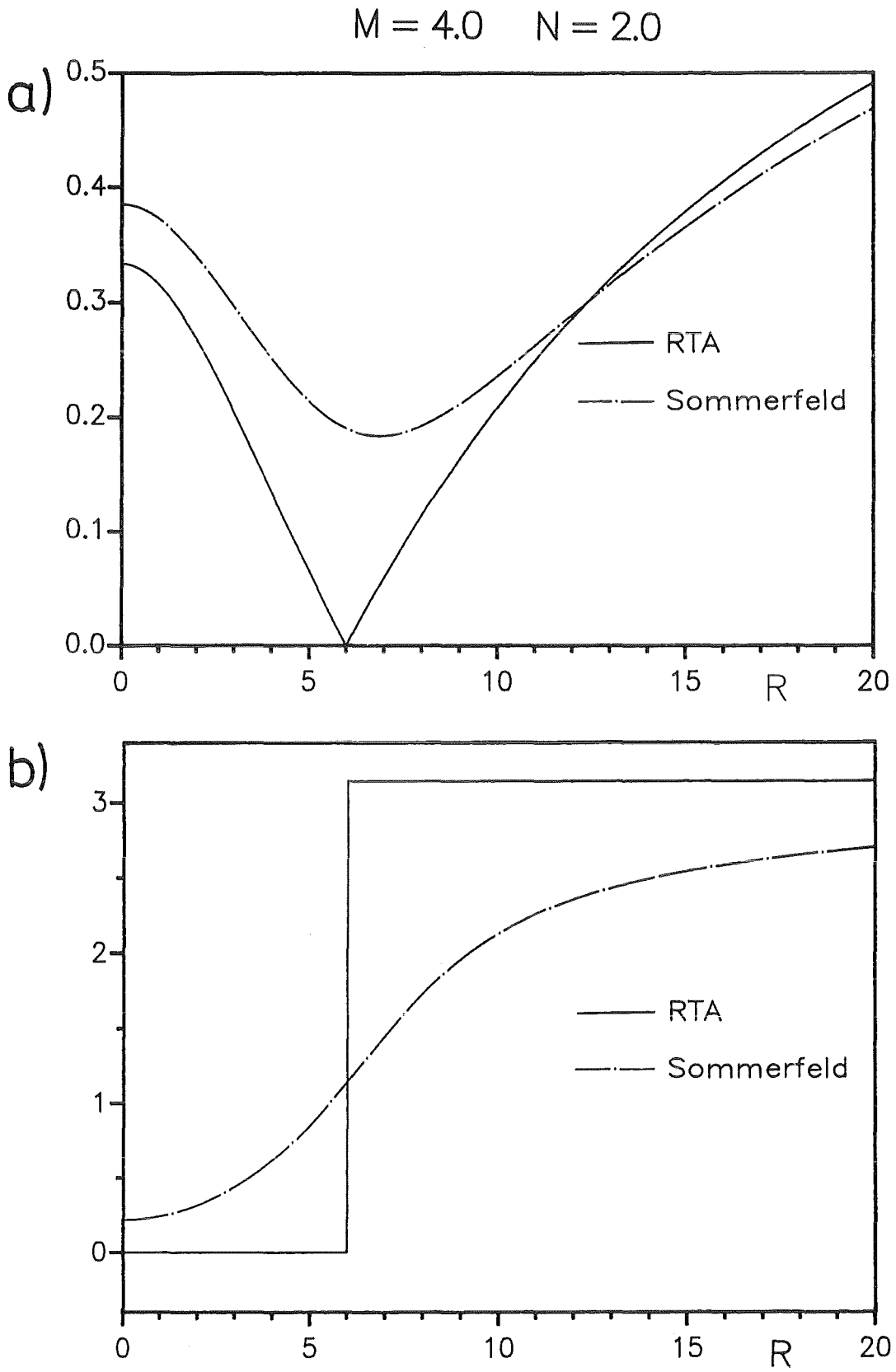

Fig.43: Magnitude (a) and argument (b) (in radian) of the local reflection coefficient for RTA and Sommerfeld waves for the ratios M and N of densities and phase velocities given above. For definition, see Eq. (6.6).

discontinuities along the line (6.3) of vanishing coefficient of local reflection. Therefor, in Fig. 41 DMRR is -1 along this line, and in Fig. 42 $D\Phi R$ has a discontinuity of π. The local reflection coefficient of the Sommerfeld wave follows smoothly the trend of the RTA wave, both in magnitude and in argument as shown in Fig. 43. For this figure, ΦR_{RTA} has been increased by 2π for Z values which are smaller than those given by Eq. (6.3).

7. Summary

In this report we have described the physical background of the diffraction of plane and spherical harmonic scalar waves without attenuation at the interface between two homogeneous fluids. The strict Sommerfeld complex integral formalism for spherical waves has been transformed into finite and infinite real integrals in k-spaces. 'Optical' coordinates for reflected and transmitted wave fields are discussed, including scale factors and differential operators. These coordinates are used to formulate the ray tube approximation for diffracted spherical waves.

The reliability of our algorithm is shown by comparing the Sommerfeld results (Sommerfeld waves) for the incident wave (Fig. 7) with the well known analytical form (Fig.6).

All calculations of reflected and transmitted waves concern the near field region. The point source is about half a wavelength above the diffracting plane. Sommerfeld waves for reflection and transmission are shown for the following combinations of ratios M and N of densities and phase velocities: M = 1, N = 2 (Figs. 10,11), M = 4, N = 2 (Figs. 16, 17), M = 1, N = 0.5 (Figs. 22, 23), and M = 0.25, N = 0.5 (Figs. 27, 28). The Sommerfeld waves are the sum of 'homogeneous' and 'inhomogeneous' components as defined in Subsection 3.2.1. These components are shown also.

The cases with M = 1 could be extended to describe the diffraction of electric dipole radiation, those with $M = N^2$ to describe diffraction of magnetic dipole radiation. This follows from Eq. (2.18).

The ray tube approximation (RTA) is unsuited for the cases with N < 1 where total reflection is involved. Therefore, RTA waves are shown only for the cases M = 1, N = 2 (Figs. 32, 33) and M = 4, N = 2 (Figs. 35, 36). The violation of the Helmholtz wave equation is

demonstrated for these cases in Figs. 34 and 37. RTA waves are compared with Sommerfeld waves by plotting the differences of absolute values (Figs. 38, 41) and of phase angles (Figs. 39, 42). The local reflection coefficients of RTA and Sommerfeld waves are intercompared in Figs. 40 and 43.

Two interesting features have been observed which possibly could help to find an analytical description of Sommerfeld waves:

- When a spherical wave is transmitted into an acoustically thinner medium, a ring of zero absolute sound pressure appears which absorbs an excess of phase angle of 2π. This is shown in Figs. 22 and 23 for the case $M = 1$, $N = 0.5$. To our knowledge, this effect has not yet been described in the literature.

- For the case $M = 1$, $N = 2$ there is a cone on which reflected RTA and Sommerfeld waves seem to have equal absolute values (Figs. 38 and 40a).

Further search for an analytical description of diffraction of spherical waves will be based on the results of this report.

Acknowledgements

One of the authors (Ch. W.) would like to thank Prof. P. Hubral, Universität Karlsruhe, Geophysikalisches Institut, and Prof. K. J. Langenberg, Gesamthochschule Kassel, Fachgebiet Theoretische Elektrotechnik, for clarifying discussions.

References

1. H.Fischer, Remote sensing of atmospheric trace constituents using Fourier transform spectroscopy, Ber. Bunsenges., Phys.Chem. 96 (1992) 306-314.

2. Ch.Weddigen, C.E.Blom, and M.Höpfner, Phase corrections for the emission sounder MIPAS-FT, Appl.Opt. *32* (1993) 4586-4589.

3. C.E.Blom, M.Höpfner, and Ch.Weddigen, Correction of phase anomalies of atmospheric emission spectra by the double differencing method, submitted to Appl.Opt. (June 1995).

4. A.Sommerfeld, Über die Ausbreitung der Wellen in der drahtlosen Telegraphie, Ann.Phys. *28* (1909) 435-437.

5. M.Born and E.Wolf, Principles of Optics, Sixth Edition, Pergamon Press Oxford, 1987.

6. L.M.Brekhoviskikh and O.A.Godin, Acoustic of Layered Media I, Springer-Verlag Berlin,1990, p.4 ff.

7. A.Sommerfeld, Theoretische Physik IV (Optik), Dietrich'sche Verlagsbuchhandlung Wiesbaden,1950, p.31.

8. J.J.Bowman (Editor), Electromagnetic and acoustic scattering by simple shapes, North Holland Publishing Company, Amsterdam, 1969.

9. L.M.Brekhoviskikh and O.A.Godin, Acoustic of Layered Media II, Springer-Verlag Berlin, 1992.

10. I.N.Bronstein and K.A.Semendjajew, Taschenbuch der Mathematik, Verlag Harri Deutsch, Thun, 1983.

11. R.Becker, Theorie der Elektrizität, Verlag von B.G.Teubner, Berlin, 1944.

12. CA-DISSPLA, Version 11.0, Computer Associates International Inc., New York, 1989.